Development and Testing of an Integrated Liquid-Fuel-Injector/Plasma-Igniter for Scramjets

Cody Dean Anderson

Thesis submitted to the faculty of the
Virginia Polytechnic Institute and State University
in partial fulfillment of the requirements for the degree of

Master of Science
In
Aerospace Engineering

J.A. Schetz, Chair
W.F. O'Brien
L.S. Jacobsen

February 13, 2004
Blacksburg, Virginia

Keywords: Liquid Injection, Scramjets, Penetration, Atomization, Plasma Torch

Development and Testing of an Integrated Liquid-Fuel-Injector/Plasma-Igniter for Scramjets

Cody Dean Anderson

(ABSTRACT)

A newly designed liquid fuel (kerosene) aeroramp injector/plasma igniter was tested in cold flow using the Virginia Tech supersonic wind tunnel at Mach 2.4. The liquid fuel (kerosene) injector is flush wall mounted and consists of a 2 hole aeroramp array of impinging jets that are oriented in a manner to improve mixing and atomization of the liquid jets. The two jets are angled downstream at 40 degrees and have a toe-in angle of 60 degrees. The plasma torch used nitrogen and air as feedstocks and was placed downstream of the injector as an ignition aid. First, schlieren and shadowgraph photographs were taken of the injector flow to study the behavior of the jets, shape of the plume, and penetration of the liquid jet. The liquid fuel aeroramp was found to have better penetration than a single, round jet at 40 degrees. However, the liquid fuel aeroramp does not penetrate as well as an upstream/downstream impinging jet in a plane aligned with the flow. Next, the Sauter mean droplet diameter distribution was measured downstream of the injector. The droplet diameter was found to vary from 21 to 37 microns and the atomization of the injector does not appear to improve beyond 90 effective jet diameters from the liquid fuel aeroramp. These results were then used to decide on an initial location for the plasma torch. The combined liquid injector/plasma torch system was tested in an unheated (300 K) Mach 2.4 flow with a total pressure of 345 kPa. The liquid fuel (kerosene) volumetric flow rate was varied from 0.66 lpm to 1.22 lpm for the combined liquid injector/plasma torch system. During this testing the plasma torch was operated from 1000 to 5000 watts with 25 slpm of nitrogen and air as feedstocks. The interaction between the spray plume and the plasma torch was observed with direct photographs, videos, and photographs through an OH filter. It is difficult to say that any combustion is present from these photographs. Of course, it would be surprising if much combustion did occur under these cold-flow, low-pressure conditions.

Differences between the interaction of the spray plume and the plasma torch with nitrogen and air as feedstocks were documented. According to the OH wavelength filtered photographs the liquid fuel flow rate does appear to have an effect on the height and width of the bright plume. As the liquid fuel flow rate increases the bright plume increases in height by 30% and increases in width slightly (2%). While, a decrease in liquid fuel flow rate resulted in an increase in height by 9% and an increase in width by 10%. Thus, as the liquid fuel flow rate varies the width and height of the bright plume appear to always increase. This can be explained by noticing that the shape of the bright plume changes as the liquid fuel flow rate varies and perhaps anode erosion during testing also plays a part in this variation of the bright plume. From the OH wavelength filtered photographs it was also shown that the bright plume appears to decrease in width by 9% and increase in height by 22% when the plasma torch is set at a lower power setting. When air is used as the torch feedstock, instead of nitrogen, the penetration of the bright plume can increase by as much as 19% in width and 17% in height. It was also found that the height and width of the bright plume decreased slightly (2%) as the fuel flow rate increased when using air as the torch feedstock. Testing in a hot-flow facility is planned.

List of Tables

List of Figures

Nomenclature

A = area

C_d = discharge coefficient

CF = correction factor

D_{32} = Sauter mean droplet diameter

d_{eq} = equivalent jet diameter

d_{eff} = effective jet diameter

d_{iris} = diameter of the iris on the digital camera

f = focal length

f-stop = ratio of the focal length to the iris diameter

λ = wave length

M = mach number

P = pressure

P_{eb} = effective back pressure

P_{exit} = exit pressure

$P_{0,\infty}$ = freestream stagnation pressure

$\bar{q}$ = jet to freestream momentum flux ratio

Q = volumetric flow rate

ρ = density

SMD_m = measured sauter mean diameter

SMD_0 = corrected sauter mean diameter

T = transmission

$T_{0,\infty}$ = freestream stagnation temperature

θ = scattering angle

U = velocity

ULDF = upper limit distribution function

Subscripts

o = stagnation

∞ = freestream

j = jet

Table of Contents

Chapter 1: Introduction

Scramjet combustion is a difficult and daunting task to tackle. Among other problems there is the difficulty in mixing and ignition of fuel, especially hydrocarbons in a supersonic flow. The application of gaseous or liquid hydrocarbon fuels to scramjets has been studied on and off for about 50 years. Researchers at Fairchild, United Technologies, Applied Physics Laboratory of Johns Hopkins University, Air Force Research Labs and others in the US and overseas have contributed to this effort. A few representative examples of relatively recent studies are in References [1] – [6].

Extensive research has been done at Virginia Tech regarding fuels and combustion for the purpose of supersonic combustion. One approach to this problem is to break up the combustion system and study the mixing and ignition separately. Once everything is known about the individual systems, then they are combined to create a viable combustion system. This design approach has continued to be the preferred approach at Virginia Tech and elsewhere.

A substantial amount of research has been performed in the field of gas injection in supersonic flows. This research has included techniques such as: transverse injection,[7-12] slots,[7, 8, 13] ramps,[14-15] and jet swirl.[7, 8, 16-19] This work is reviewed and summarized in Schetz et al.[7] At Virginia Tech, a gas injection system, known as the aeroramp, was created based on this research.[20-22] The aeroramp involves an array of angled jets that induces additional vorticity and enhances mixing.

There is also a large body of research on liquid injection in supersonic flow, with a significant fraction performed at Virginia Tech. This research includes studies on penetration and mixing,[23-26] along with the effects of properties and location in the plume on the mean droplet diameter.[27-29] Studies have also been done on various types of complex injectors such as impinging jets.[30] The impinging jets in Ref. [30] were angled upstream and downstream at 60 degrees to the wall and lay in a plane perpendicular to the wall. The impinging jets were spaced at $s/d_{eq} = 5.0$.

An important component of a supersonic combustion system is the ignition aid. It is difficult to ignite either a gas or liquid hydrocarbon in a supersonic flow. At Virginia Tech, we have decided to use a plasma torch to overcome these difficulties. Over the

years, we and others have done considerable research using plasma torches as an ignition aid.[31-35]

Based on this plasma torch research and research done using gas injection it was decided to create a combined aeroramp/plasma torch injector/ignition system as a viable scramjet combustion system.[21, 22] This combined aeroramp/plasma torch ignition system was tested in a cold flow facility at Virginia Tech at Mach 2.4 with gaseous ethylene fuel and was proved to have a good potential as a solution for supersonic combustion. Currently, this system is being tested in a hot flow facility at the University of Virginia. By testing in a hot flow facility, one can more accurately simulate the temperature ranges that would normally been seen in a supersonic combustion chamber.

At present, the plan for the X-43C flight test vehicle for cold-start combustion is to use silane as an ignition aid. Silane is a dangerous gas that ignites upon contact with oxygen. Because of the dangers of this setup, it was decided that another solution needed to be explored for cold-start combustion. The next idea was to use JP7 for both cold-start combustion and normal combustion on the X-43C. The concept is to cold-start the engines with liquid JP7 and to circulate the liquid JP7 through the airframe for cooling purposes. Over time, the liquid JP7 would then be heated up due to the flow around the airframe and the liquid would then be cracked into a gas for subsequent combustion. This gas could then be used as the main combustion source. In order for this to work, a combined liquid and gas injection system with an effective ignition aid must be designed.

At Virginia Tech, it was decided that the liquid injection system should be an impinging jet/aeroramp design based on the work previously done by Hewitt[30] and Jacobsen[21], respectively. The impinging jets would help create more atomization of the liquid jets, while the aeroramp induces additional vorticity and mixing. This system would in essence create a liquid fuel aeroramp. The liquid fuel aeroramp consists of an array of liquid jets that are angled downstream and then toed in towards each other based on past research.

The injector system was designed and preliminary evaluations were conducted using water in a cold-flow supersonic facility at Mach 2.4. The injector was tested to make sure that the jets did in fact impinge while being swept downstream and toed in towards each other as was originally intended. After the jets were proven to work as planned, the

remainder of the study was done using kerosene as a safer and readily available alternative to JP7 fuel. Shadowgraphs and schlieren photographs were taken. Using these photographs, the penetration of the jet was estimated in order to lay out a grid for droplet size measurement. Sauter mean droplet size, D_{32}, measurements were taken using a Rayleigh scattering technique similar to that used by Hewitt.[30] The kerosene injector was then combined with a plasma torch in order to create a viable scramjet engine combustion system. The preliminary location of the plasma torch was chosen based on the droplet size measurements. The interactions between the spray plume and the plasma torch were observed with direct photographs, videos, and photographs through an OH filter.

Chapter 2: Test Facilities

2.1 Virginia Tech Supersonic Wind Tunnel

The experiments took place in the Virginia Tech 23 x 23 cm blowdown supersonic wind tunnel. This tunnel was designed and built at NASA Langley Research Center and acquired by Virginia Tech in 1958. For these experiments, the tunnel was configured with a convergent-divergent nozzle that resulted in a freestream Mach number of 2.4. The test section dimensions were 23 cm wide x 23 cm high x 30 cm long in the streamwise direction. During a representative run the measured freestream stagnation pressure, $P_{0,\infty}$, and temperature, $T_{0,\infty}$, were 345 kPa and 292 K, respectively. Figure 2.1 shows a sketch of the wind tunnel test arrangement. The typical run time for the tunnel in this experiment was seven seconds.

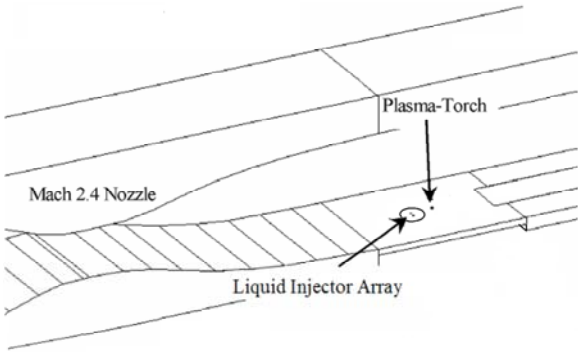

Figure 2.1 Tunnel setup with injector and plasma torch[21]

2.2 Data Acquisition

Analog signals from the pressure transducers and thermocouples were through a National Instruments AMUX-64T multiplexor board to a personal computer via a National Instruments AT-MIO-16XE-50 multifunction high speed analog/digital I/0 board. The AT-MIO-16XE-50 was operated in 32 channel differential mode. The measured data was then recorded using LabView software. The tunnel and measurement devices were all controlled and run using LabView.

Chapter 3: Liquid Fuel Injector

3.1 Liquid Injector Requirements

The liquid injector was designed by looking at the advantages of impinging liquid jets and combining them with the advantages of an aeroramp. In designing the injector a momentum flux ratio, $\bar{q}$, around 5-10 was selected for good penetration,[26] where:

$$\bar{q} = \frac{(\rho U^2)_j}{(\rho U^2)_\infty} \tag{3.1}$$

It was decided that the angles from the gaseous fuel aeroramp should be made the same in the liquid injector and the fuel flow rate should be matched as closely as possible to the earlier gaseous fuel aeroramps[21] in order to take advantage of the improved mixing found there. The liquid injector was designed to have a volumetric flow rate of 1.37 lpm. By fixing these requirements, the number of holes, jet diameter, and angles were determined. The liquid injector consisted of two holes, each 0.533 mm in diameter. Two holes were used in the liquid fuel aeroramp array rather than the nine[20] or four[21] holes used for gaseous fuel aeroramp arrays because the higher density of liquids which leads to very small holes. These holes were spaced 4.34 mm apart ($s/d_{eq} = 5.76$), while being angled downstream 40 degrees and toed in 60 degrees. The spacing of the liquid jets was based off of direct photographs of the liquid aeroramp. Figures 3.1 and 3.2 show sketches and a picture of the liquid injector used in this experiment.

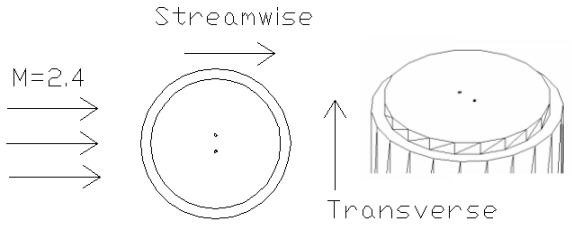

(a) Top views

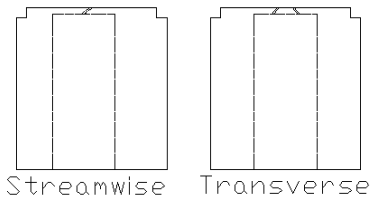

(b) Transverse sections

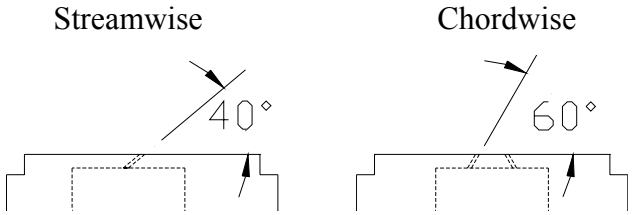

(c) Close-up of angles for liquid injector

Figure 3.1 Liquid injector layout

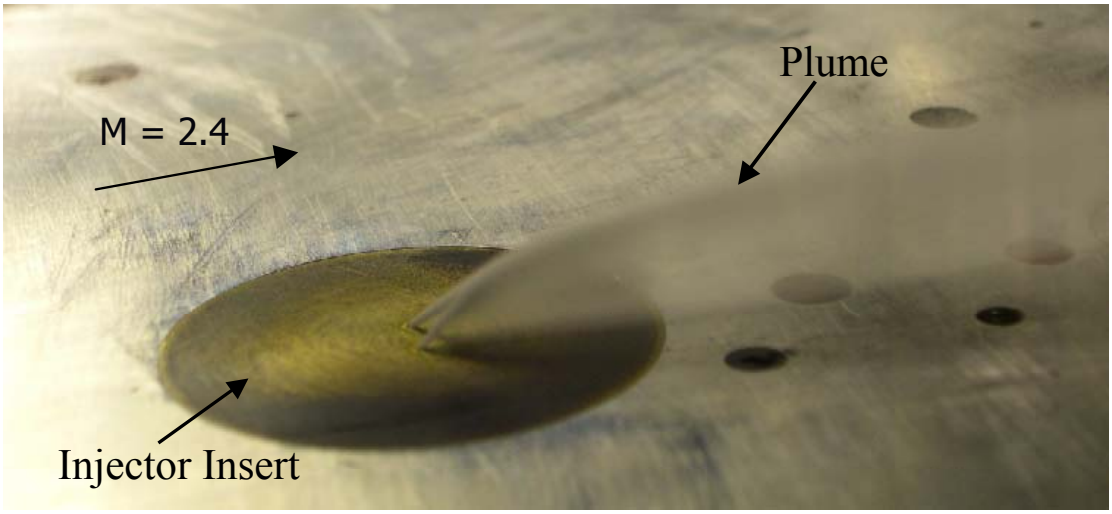

Figure 3.2 Liquid injector in Mach 2.4 flow

3.2 Liquid Injection System

In order to inject the liquid into the supersonic tunnel, an injection system was needed, and a pressurized system was chosen. The pressurized system consisted of a liquid tank, used to hold reserve fuel, and a pressurizing gas which was used to force the liquid out of the tank as shown in Figure 3.3. The liquid tank was refilled using the gravity feed system shown in Figure 3.4. The liquid was poured into the funnel and into a clear braded plastic tube. The liquid then traveled into the tank by way of a valve at the bottom of the tank. The liquid then filled the tank vertically. The amount of liquid in the tank was measured by simply looking at the clear braded tubing and realizing that since this is a gravity feed system that the level inside the liquid tank would be equal to that shown in the clear tubing. It is important to note that the vent, for gas, at the top of the tank must be open in order to fill the tank. If this vent is not opened then gas will be trapped in the liquid tank, which makes filling the liquid tank much more difficult. After filling the tank the excess liquid, in the clear tubing, was drained out into a proper container via a vent located at the bottom of the tubing. Once the tank is properly filled, it can be pressurized for use during testing. The pressurized gas enters the top of the liquid tank, which then forces the liquid out of the bottom of the tank and through a particle filter on its way to a pneumatic valve. This system allowed the liquid fuel to be turned on and off through the use of a pneumatic valve located a short distance from the injector. The pneumatic valve was in turn controlled by an electrical signal from LabView via a personal computer. This allowed the user to control when the injector turned on and off while reaching a steady state pressure in the injector in a reasonably short period of time.

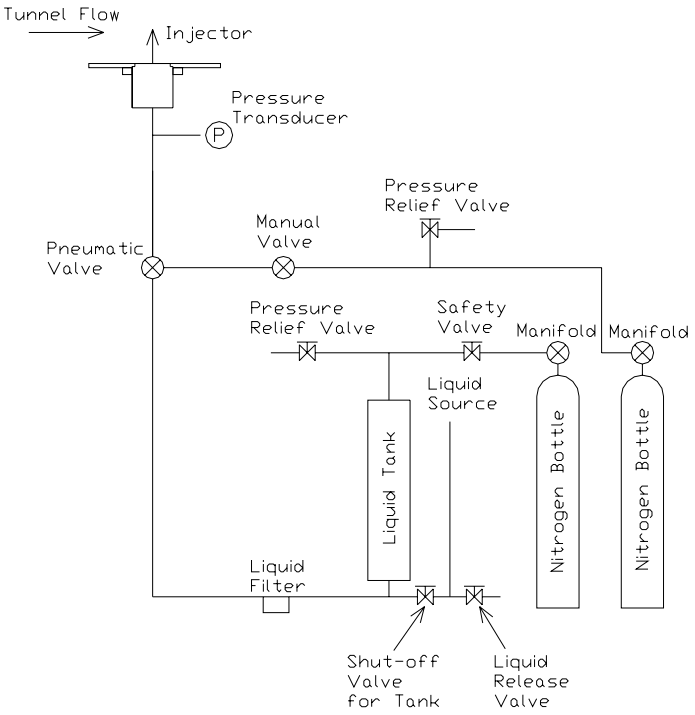

Figure 3.3 Liquid injector setup

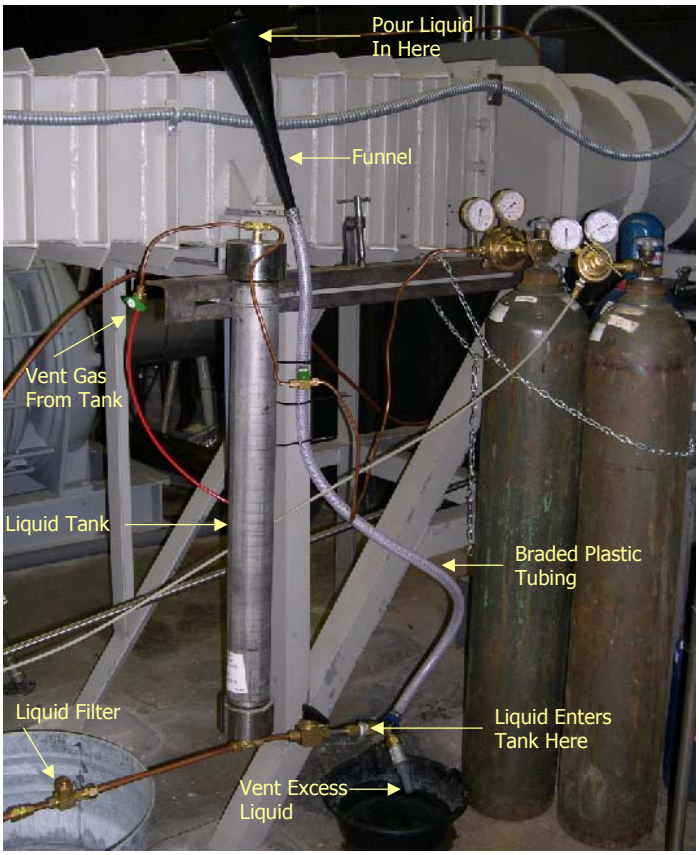

Figure 3.4 Gravity feed system for the liquid tank

3.3 Liquid Injector Calculations

Since this injector design called for a small jet diameter, which resulted in high pressure jets with a small flow rate, there was no commercial flow meter found to measure the flow accurately. When searching for flow meters it was found that several companies made flow meters for low flow rates, but they could not withstand high pressures and vice versa. For this reason it was decided that a flow meter would need to be created based on the basic concept of an orifice flow meter. The following information describes how this orifice flow meter was developed.

First, the flowrate of the injector was controlled by regulating the pressure in the liquid tank. The pressure was determined just before the injector and just on the outside of the injector. These pressures were then related by the following equation to calculate the volumetric flow rate.[36]

$$Q_j = C_d A_{eq} \sqrt{\frac{2(P_j - P_{exit})}{\rho(1-\beta^4)}} \tag{3.2}$$

where C_d is the discharge coefficient, A_{eq} is the equivalent area of the injectors, ρ is the density of the liquid, and P_j and P_{exit} are the pressures of the injector and the tunnel, respectively. Figure 3.5 is a sketch showing the nomenclature for equation 3.2. The relation for β is given as:

$$\beta = \frac{d_{eq}}{D} \tag{3.3}$$

where d_{eq} is the equivalent jet diameter and D is the diameter of the tube leading to the jet. In this case $d_{eq} << D$, therefore $\beta^4 \approx 0$ and equation 3.2 becomes:

$$Q_j = C_d A_{eq} \sqrt{\frac{2(P_j - P_{exit})}{\rho}} \tag{3.4}$$

When calculating P_{exit} in the supersonic tunnel one would like to use the effective back pressure, P_{eb},[37] where:

$$P_{exit} = P_{eb} = 0.8P_2 \tag{3.5}$$

Actually, $P_{eb} << P_j$ for our conditions, so any uncertainty in defining P_{eb} for this complex injector is unimportant. Equations (3.4) and (3.5) were then used to calculate

the volumetric flow rate, Q. The volumetric flow rate was varied during testing to study the effects of flow rate on the integrated liquid injection/plasma torch combustion system.

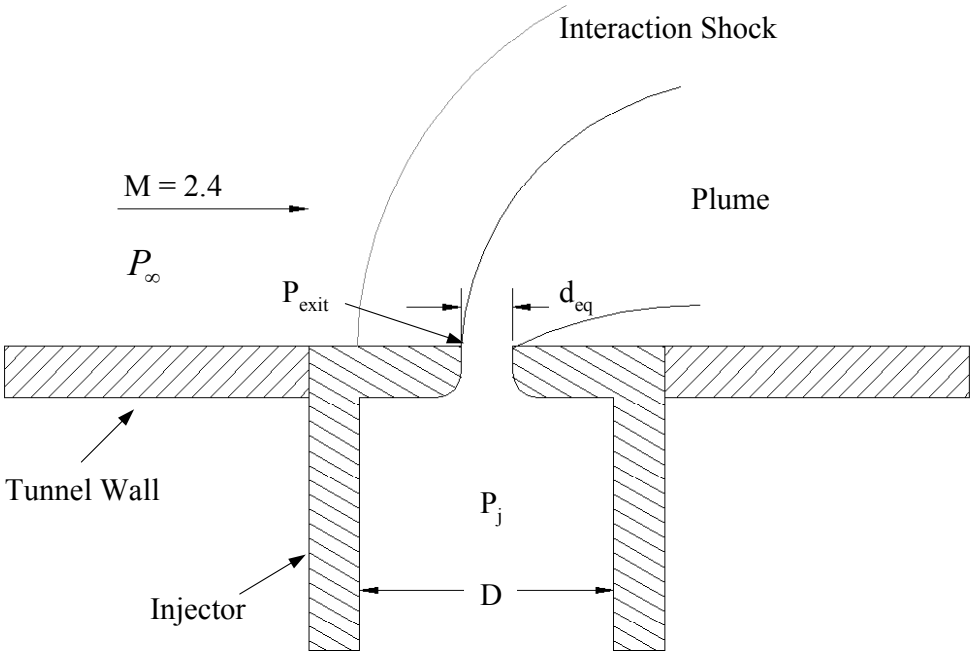

Figure 3.5 Nomenclature for volumetric flow rate calculations

The discharge coefficient was determined by injecting fluid through the injector and into a container and measuring the volume over a known time period. The injector pressure and atmospheric pressure were also recorded during this process. By using these pressures along with equation (3.4) one can then calculate the discharge coefficient. It was found that the discharge coefficient was 0.604 for the liquid fuel aeroramp. The flow rate can now be measured based on pressure measurements alone.

One can now relate the jet diameter in terms of the equivalent jet diameter:

$$d_{eq} = dj\sqrt{2} \tag{3.6}$$

and effective jet diameter:[21]

$$d_{eff} = d_{eq}\sqrt{C_d} \tag{3.7}$$

The equivalent jet diameter was 0.754 mm and the effective jet diameter was 0.586 mm.

During liquid injection testing, the pressure was typically set to 1.793×10^6 Pa. This pressure was chosen because of restrictions on the regulator for the pressurizing gas and safety concerns regarding other components of the liquid injection system. Higher

pressures could be achieved, but only for a short number of runs. Based on this pressure setting and a discharge coefficient of 0.604, the volumetric flow rate was calculated to be 1.078 lpm and the momentum flux ratio was found to be 6.0.

Based on knowledge gained through the development and testing of the liquid fuel aeroramp it might be possible to improve the discharge coefficient to a value of 0.8. If one were to assume the testing was done at the same pressure with a discharge coefficient of 0.8, then the volumetric flow rate and momentum flux ratio would be 1.43 lpm and 10.8 respectively. These values are closer to the designed volumetric flow rate and momentum flux ratio. However, based on restrictions on the equipment, as mentioned previously, one could not achieve both the designed volumetric flow rates and the momentum flux ratio without an improvement in the design and manufacturing of the liquid fuel aeroramp.

3.4 Parameter Effects

In the design of the injector one can vary several components to get the desired volumetric flow rate and momentum flux ratio. First, let us look at the momentum flux ratio. One can calculate the velocity of the liquid, U, from the volumetric flow rate by using the following relation:

$$U = \frac{Q_j}{A_{eq}} \tag{3.8}$$

where A_{eq} is the equivalent area of the jet. Now going back to equation 3.4, we get:

$$U = \frac{C_d A_{eq} \sqrt{\frac{2(P_j - P_{exit})}{\rho}}}{A_{eq}} = C_d \sqrt{\frac{2(P_j - P_{exit})}{\rho}} \tag{3.9}$$

Knowing that a liquid jet is incompressible and using equations (3.9) and (3.1) we get:

$$\overline{q} = \frac{(\rho U^2)_j}{(\gamma P M^2)_\infty} = \frac{(\rho \left\{ C_d \sqrt{\frac{2(P_j - P_{exit})}{\rho}} \right\}^2)_j}{(\gamma P M^2)_\infty} \tag{3.10}$$

The momentum flux ratio is independent of the equivalent area of the jet. However, the volumetric flow rate is directly related to the diameter of the jet and thus

the equivalent area. By going back and looking at equations (3.10) and (3.4) one can see that changing the discharge coefficient will improve both the momentum flux ratio and the volumetric flow rate.

Chapter 4: Plasma Torch

A DC plasma-torch was operated from 1000 to 5000 watts with nitrogen and air as feedstocks (see Figure 4.1). The torch feedstock flow rate was set at 25 slpm while running chamber pressures between 40 and 50 psig. This is the same torch as used by Gallimore et al.[22] at Virginia Tech and similar in principle to other plasma torches used here in the past.[31-33]

The plasma-torch cathode was made out of 2% thoriated tungsten with a 20 degree half angle cut at both ends of the cathode and the anode was made of copper. The throat diameter of the anode started at 1.59 mm and gradually increased in size as erosion took place during testing. The gap between the cathode and anode was set to 1.02 mm using a Starret micrometer that was directly connected to the cathode.

Three Miller SR-150-32 arc welders were linked in series to provide the DC power to the plasma-torch. A Miller HF-251D-1 high frequency electric starter was used to initiate the electric arc for the plasma torch, while the output of the power supply was measured by using a 50A/50mV shunt and voltage divider/isolator board. A gas cylinder that was connected to the torch via a Sierra 840M orifice flow meter and Sierra 902C digital dual channel flow controller provided the feedstock gas.

For the original gaseous fuel aeroramp/plasma torch igniter, the plasma-torch was located at 28.6 mm, 38.1 mm, and 47.6 mm from the center of the 4 hole injector array.[21] This corresponds to 6, 8 and 10 equivalent jet diameters for that injector. Jacobsen et al.[21] determined that locating the plasma torch 38.1 mm from the plasma torch was the best of the three locations. For the liquid injector/plasma igniter, the plasma torch was initially set at a distance of 65.4 mm from the injector or 112 effective jet diameters from the plasma torch. The reason that the torch location is so different for the liquid injector is that it was believed that more time/distance is needed for the jets to properly atomize. By locating the plasma torch farther from the liquid fuel (kerosene) aeroramp one should get a better atomized flow and possibly better conditions for combustion.

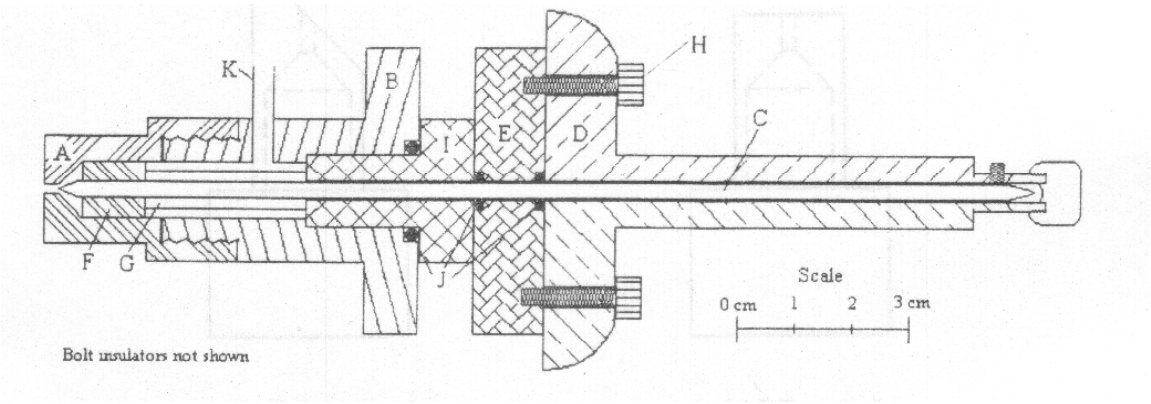

A - Anode
B - Torch Body
C – Cathode
D – Depth Micrometer
E – Cathode Assembly
F – Flow Swirler
G – Cathode Insulator
H – Bolts
I – Electric Isolator and Insulator
J – O-Rings
K – Feedstock Inlet Tube

Figure 4.1 Drawing of the Virginia Tech plasma torch[38]

Chapter 5: Instrumentation and Test Procedures

5.1 Schlieren and Shadowgraphs

Liquid jets tend to be unsteady at a very high frequency.[29] Because of this, it is useful to take both short and long exposure photographs to see what is happening instantaneously and as a time average.

Spark shadowgraphs and schlieren photographs were taken using a GenRad Strobotac type 1538-A and Xenon Model 437B Nanopulser, respectively. The exposure time of the Strobotac was approximately 10^{-6} seconds, while the exposure time for the Nanopulser was approximately 10^{-8} seconds. The schlieren (10^{-6} sec. exposure) and shadowgraph (10^{-6} sec. and 10^{-8} sec. exposure) photographs were both taken using Polaroid type 57 film.

In taking these photographs the light source was located on the near side of the tunnel while the Polaroid camera was located on the far side of the tunnel. The light source was directed away from the tunnel, through a slit and towards a concave mirror (see Figure 5.1). The mirror was then used to redirect the light through the tunnel. Careful attention was paid to aligning the light source as close as possible to being in the path of the light coming back through the tunnel. This was done to reduce the angle between the light source and the light from the mirror as much as possible. The diameter of the beam and location of the beam was also accounted for to get a column of light through the tunnel. Once the light went through the tunnel it was then reflected off a flat mirror and another concave mirror towards the camera. A knife edge was placed between the concave mirror and the camera to take schlieren photographs. This optical system was focused by placing a flashlight on the tunnel floor plate, while exposing the bulb of the flashlight. Once the system was adjusted for clarity the system was checked for reflections due to the floor plate. A screw and a swagelock male/male adapter of known dimensions were placed on top of the injector in the tunnel as a reference. From these two items one could see if there was in fact a double image where the items touched the floor plate. If a double image was seen it meant that the light source and mirror were not aligned properly in the vertical direction. This was easily corrected by traversing the light source vertically until the double image went away. This process was used each time in order to reduce any negative effects in the image due to the optical system.

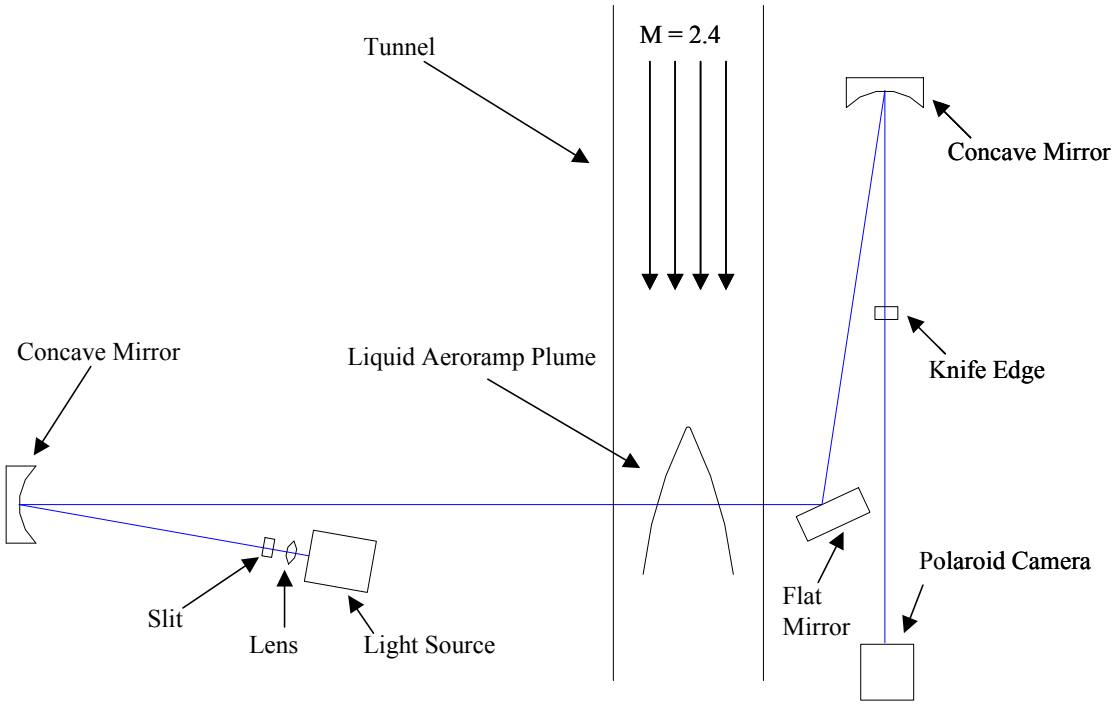

Figure 5.1 Schlieren photography setup

Shadowgraphs were also taken with a digital camera with an exposure time of 1 second in order to get a time-averaged photograph of the injector to estimate the penetration height. Only the light source and first concave mirror on the near side of the tunnel were needed for the 1 second exposure shadowgraphs. A ground piece of glass was then placed on the tunnel window on the far side of the tunnel and photographs were taken of the images shown on the ground glass.

Direct photographs and videos were taken of the liquid injector alone and the combined liquid injector/plasma torch system using a Nikon Coolpix 4300 digital camera. Additional videos were recorded using a Panasonic PK-972 video camera, but they were only used as a backup for the videos taken using the Nikon digital camera. These photographs and videos were taken to visually study the liquid injector by itself and the combined liquid injector/plasma torch system.

5.2 Droplet Measurements

5.2.1 Methods

Droplet measurements were made using a laser and a forward scattering technique.[27-30, 39-41] The forward scattering technique involves measuring the intensity of a light source alone and then recording the forward scatter of the light due to spherical droplets. This intensity profile can be characterized by a theoretical illumination profile, which should be valid for all forward scattering techniques as long as the droplets are roughly spherical in shape. By using two shape parameters as described in References [39] – [41] one can calculate the theoretical intensity of the light and the corresponding droplet diameter. The droplet diameter is calculated by using these shape parameters along with the upper limit distribution function, ULDF[41], to determine the volume-to-area mean diameter also known as the Sauter mean diameter or D_{32}[39-40]. The theoretical illumination profile, as described by Roberts and Webb[40], is shown in Figure 5.2. In this figure $I(\bar{\theta})$ is the illumination normalized with the centerline value. Hence,

$\bar{\theta} = \dfrac{\pi \ D_{32} \ \theta}{\lambda}$ is the reduced angle, where θ is the scattering angle, D_{32} is the mean droplet diameter relating volume and area of spherical droplets, and λ is the wavelength of the light.

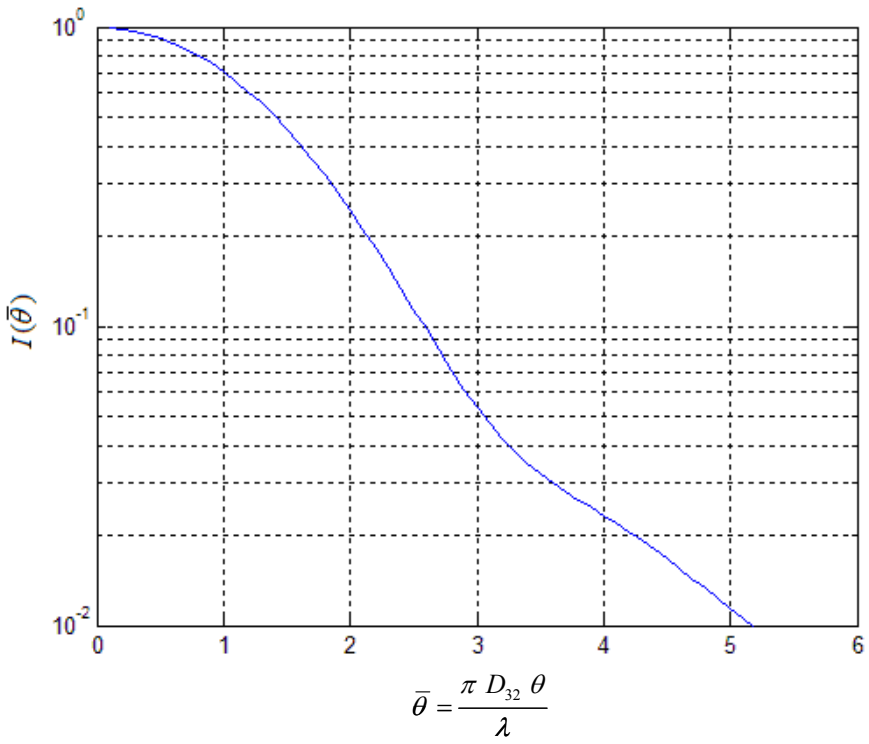

Figure 5.2 Mean theoretical illumination profile

This technique usually involves measuring the background intensity profile of the laser, windows, etc. and subtracting that from the forward scatter intensity profile due to the droplets in order to get the Sauter mean diameter, D_{32}. The new intensity profile would then be used to extrapolate out the intensity at the centerline, I_0. The centerline intensity is used to normalize all of the new intensities, and the corresponding scattering angles can be calculated based on the experimental setup. This information could then be used along with Figure 5.2 to determine D_{32}. However, this technique is not useful when dealing with a large amount of multiple scattering or absorption. If a large amount of absorption or multiple scattering takes place, then the intensities near the centerline are much lower for the measured forward scatter than they were for the background intensities. If one were to subtract the background from the forward scatter the results might in fact be negative intensities. This means that a different technique is needed for this situation. Due to the nature of the liquid injector used in this study, many droplets were concentrated in a small area near the injector. High scattering and absorption were then created due to this high concentration of droplets, so the technique was modified.

According to Roberts and Webb[40] the standard deviation from the mean decreases as the reduced angle, $\bar{\theta}$, approaches 3.0. A fourth-order polynomial was used to approximate the theoretical ULDF distribution for reduced angles between 2.0 and 5.0.[40] Using this fourth-order polynomial, two points were taken from the measured scattered light illumination profile, and simultaneous equations were solved in order to get the droplet size without having to account for the intensity at the centerline. First, the equation for the fourth-order polynomial is found from the fit of the theoretical illumination profile and recorded using the following notation:

$$I(\bar{\theta}) = \frac{I}{I_0} = P_1\bar{\theta}^4 + P_2\bar{\theta}^3 + +P_3\bar{\theta}^2 + P_4\bar{\theta} + P_5 \tag{5.1}$$

where P_1 through P_5 are known values based on the fourth-order polynomial curve fit, I is the measured intensity, and I_0 is the intensity at the centerline. Looking at equation 5.1 one can take the reduced angle, $\bar{\theta}$, and rewrite it as:

$$\bar{\theta} = \frac{\pi\ \theta\ D_{32}}{\lambda} = \frac{\pi\ \theta}{\lambda} D_{32} = \Theta\ D_{32} \tag{5.2}$$

Now, by using equations 5.1 and 5.2 and choosing two data points, as a set, from the measured profile one can develop the following equation:

$$\bar{I} = \frac{I_1}{I_2} = \frac{P_1\Theta_1{}^4 D_{32}{}^4 + P_2\Theta_1{}^3 D_{32}{}^3 + P_3\Theta_1{}^2 D_{32}{}^2 + P_4\Theta_1 D_{32} + P_5}{P_1\Theta_2{}^4 D_{32}{}^4 + P_2\Theta_2{}^3 D_{32}{}^3 + P_3\Theta_2{}^2 D_{32}{}^2 + P_4\Theta_2 D_{32} + P_5} \tag{5.3}$$

Grouping terms and rewriting the equation:

$$\underbrace{\left(\bar{I}\ \Theta_2{}^4 - \Theta_1{}^4\right) P_1}_{K_4}\ D_{32}{}^4 + \underbrace{\left(\bar{I}\ \Theta_2{}^3 - \Theta_1{}^3\right) P_2}_{K_3}\ D_{32}{}^3 + \underbrace{\left(\bar{I}\ \Theta_2{}^2 - \Theta_1{}^2\right) P_3}_{K_2}\ D_{32}{}^2$$

$$+ \underbrace{\left(\bar{I}\ \Theta_2{}^1 - \Theta_1{}^1\right) P_4}_{K_1}\ D_{32}{}^1 + \underbrace{\left(\bar{I}\ -1\right) P_5}_{K_0} = 0 \tag{5.4}$$

The final equation then becomes:

$$K_4\ D_{32}{}^4 + K_3\ D_{32}{}^3 + K_2\ D_{32}{}^2 + K_1\ D_{32} + K_0 = 0 \tag{5.5}$$

where all values of K_i are known based on the fourth-order polynomial approximation along with the measured intensity and calculated scattering angle for the two chosen data

points. The only unknowns now are the values for D_{32}, which can be solved for using a basic equation solver. When selecting data points, an attempt was made to try and choose points which resulted in a reduced angle of approximately 3.0 in order to reduce the standard deviation by as much as possible.

During the measurement process it is often noted that large amounts of multiple scattering and absorption are taking place due to the injector. This is indicated by the overall loss in intensity of the light due to the injector. According to Dodge[42] a correction factor can be applied to the droplet size measurements for liquid injectors, which cause multiple scattering. This is done by relating the corrected droplet size, SMD_0, to the measured droplet size, SMD_m, as follows:[42]

$$SMD_0 = \frac{SMD_m}{CF} \tag{5.6}$$

where SMD is the sauter mean diameter (or D_{32}) and CF is the correction factor. The correction factor can then be calculated by using a general correlation for a range of SMD between 20 and 60 microns.[42] This correlation is as follows:

$$CF = 1 - 0.9456 \quad \exp(-3.811 \ T) \quad \exp(-0.0204 \ SMD_o) \tag{5.7}$$

where T is the transmission. The transmission is simply a ratio between the centerline intensity without the droplets and the centerline intensity with the droplets. This can also be thought of as the percentage of centerline intensity lost due to the droplets. Since both equation 5.6 and 5.7 depend on SMD_0 it is necessary to iterate this equations to determine the final corrected droplet size in microns. According to Dodge[42] this correlation fits the actual data with an R^2 value (square of the correlation coefficient) of roughly 0.92. This means that this correlation was a reasonably good fit for the data studied by Dodge.[42] Therefore, this correlation should be reasonably accurate for correcting our particular data set.

5.2.2 Measurement System

In order to measure the droplet size, D_{32}, of the liquid injector a series of equipment was needed as shown in Figure 5.3. The Spectra-Physics Stabilite model 120 helium-neon laser was placed on one side of the supersonic tunnel, while the GARRY 3000 CCD was placed on the other side of the tunnel. The 15 mW laser beam was first

aligned such that it went through a JODON LPSF-100 spatial filter in order to clean up the beam. The beam then traveled through the JODON BET-25 beam expanding telescope to collimate the beam. After the beam was collimated, it was sent through a simple camera iris. The iris was used to control the size of the beam and was carefully adjusted to make a circle, which resulted in a beam diameter of approximately 2 mm. Once the beam was adjusted to the proper size it was then redirected through a series of flat mirrors used as beam steerers. These beam steerers were set up such that the entire system could be translated horizontally and the top mirror could be adjusted vertically. This system allows one to move the beam downstream of the injector and vertically across the plume of the injector. After the beam went through the beam steerers, it was then aimed through the tunnel and towards the CCD. On the other side of the tunnel, a plano-convex lens with a focal length of 500 mm, was used to collect the scattered light created by the liquid injector. The plano-convex lens then collimated the beam once again on its way to the CCD. The CCD measures the light intensity along its array of pixels.

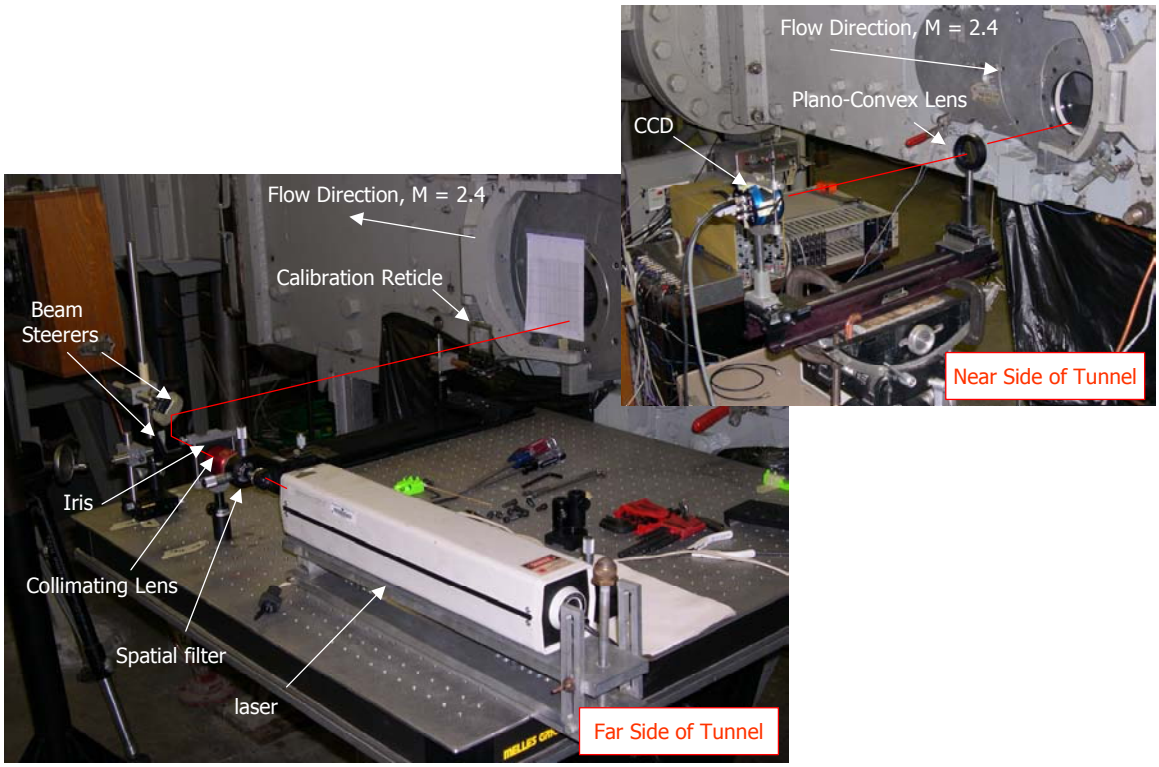

Figure 5.3 Equipment used for droplet measurement

The light enters into the CCD where the device can measure the light intensity and then display the intensities on a personal computer using Spectra Array version 2.11 by Lastek Pty. Ltd via a LAD-1250 PCI data acquisition and controller board by Ames Photonics Inc. This program is then used to take both instantaneous and time average measurements of the light intensity. An important thing to note is that aiming the laser beam directly into the CCD is effectively useless, because the intensity of the laser beam is much higher than the measurable intensity that the CCD can handle. For this reason, the laser beam needs to be aimed slightly to the side of the CCD and this distance is recorded as the shift as noted in Figure 5.4.

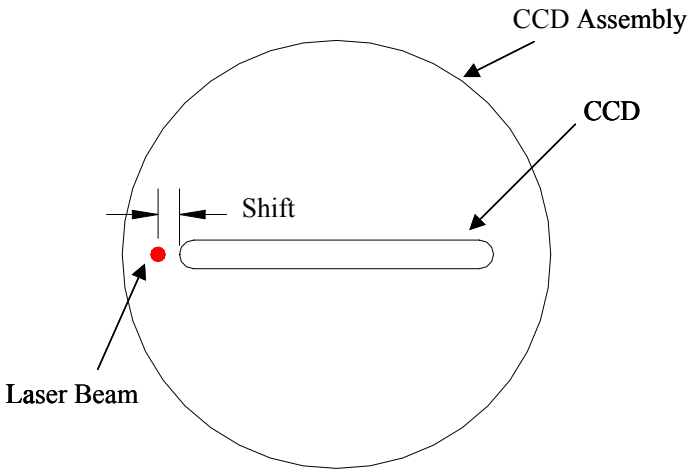

Figure 5.4 Sketch of the CCD showing the shift of the laser beam

First, the location in terms of pixels needs to be converted to scattering angles in order for the measured light intensities to be useful in determining the droplet sizes. This is done by noting that for this particular CCD there is 1 pixel every 7 μm. The focal length, *f*, of the plano-convex lens and the wavelength, λ, of the helium-neon laser also need to be noted. The next step is to convert each pixel to a reduced angle by using the following equation:

$$x_{mm} = shift + pixel \frac{7}{1000} \tag{5.8}$$

Where x_{mm} is the distance in terms of mm, "shift" is measured in mm as shown in Figure 5.4, and "pixel" is the pixel number on the CCD as displayed in the spectra array program. By using trigonometry one can now find θ as:

$$\theta = \tan^{-1}\left(\frac{x_{mm}}{f}\right) \tag{5.9}$$

Going back to equation 5.2, the value for Θ is found as:

$$\Theta = \frac{\pi\ \theta}{\lambda} \tag{5.10}$$

where the scattering angle is independent of D_{32} as shown in equation 5.2. By using equations 5.1-5.5 and 5.8-5.10 one can now choose two data points and solve for D_{32} independently from the center line intensity as was required by previous forward scattering methods.

When setting up the optical system, a calibration reticle was used to check the calibration of the measured intensities. The calibration reticle, RR-50.0-3.0-0.08-102 by Laser Electro-Optics, was based on the concept of a Rosin-Ramler distribution.[42-44] This particular distribution resulted in Sauter mean diameters, D_{32}, ranging from approximately 45 to 60 microns depending on where the laser beam was located on the reticle. One should note that, according to the fundamental equations, the mean value for D_{32} on the calibration reticle was 55 microns.

5.3 Filtered Photography

An OH filter was placed over the end of a Nikon Coolpix 4300 digital camera, and photographs were taken of the liquid injector/plasma torch combination. The OH filter allows light with the same wavelength as OH to pass through the filter. It is important to note that the fused silica supersonic tunnel windows allowed ultraviolet light to pass through them and thus should not have an effect on the OH filtered photography. In principle by using an OH filter it can be determined if combustion is present, since OH is an important component of combustion. Unfortunately, it is difficult to determine if combustion is in fact present through the use of an OH filter alone, since there is a possibility that other light with the same wavelength can also pass through this filter. This technique was only used as a quick way to determine if any combustion could be present in the cold, supersonic flow before deciding what the next step should be in exploring this liquid injector/plasma torch setup in preparation for hot-flow tests.

Chapter 6: Results and Analysis

6.1 Schlieren and Shadowgraphs

Schlieren and shadowgraph pictures were taken of the liquid injector alone in a Mach 2.4 flow, and some are shown in Figure 6.1. The flow in these pictures goes from right to left. Figure 6.1 indicates that the jets cause a weak shock wave, which will result in a low total pressure loss. These photographs were also used to measure the penetration height of the liquid injector in order to lay out a grid for droplet size measurements.

When looking at Figure 6.1, one might notice that more light passes through the plume of the injector for the 10^{-8} sec. shadowgraph and the 10^{-6} schlieren than it does for the other two. Part of the reason for this is that a strobotac was used for the 10^{-6} sec. and 1.0 sec shadowgraphs, while a nanopulser was used for the 10^{-8} sec. shadowgraph photograph. A strobotac was also used for the 10^{-6} sec. schlieren photograph. Differences in the light source and technique give the false appearance that there is more atomization in the top two pictures than in the bottom two of Figure 6.1. It should also be noted that the top three photographs in Figure 6.1 were taken closer to the injector than the bottom photograph. The reason for this is that in the top three photographs one is more interested in what is going on right around the injector. While, in the bottom photograph one is mainly interested in measuring the penetration height at multiple downstream locations.

In studying the photographs in Figure 6.1 one should note that the top three photographs were taken as a spark photographs, meaning that the light source was triggered from a remote location for a single flash while leaving the film exposed. While, the bottom photograph in Figure 6.1 was taken by adjusting a strobotac such that it was an effectively constant light source. A piece of ground glass was then placed on the far side tunnel window, and a photograph was taken using a one second exposure on a digital camera. The lines in the middle of each photograph are in fact scratches on the glass and should not be confused as shock waves or any other effects in the flow due to the liquid aeroramp.

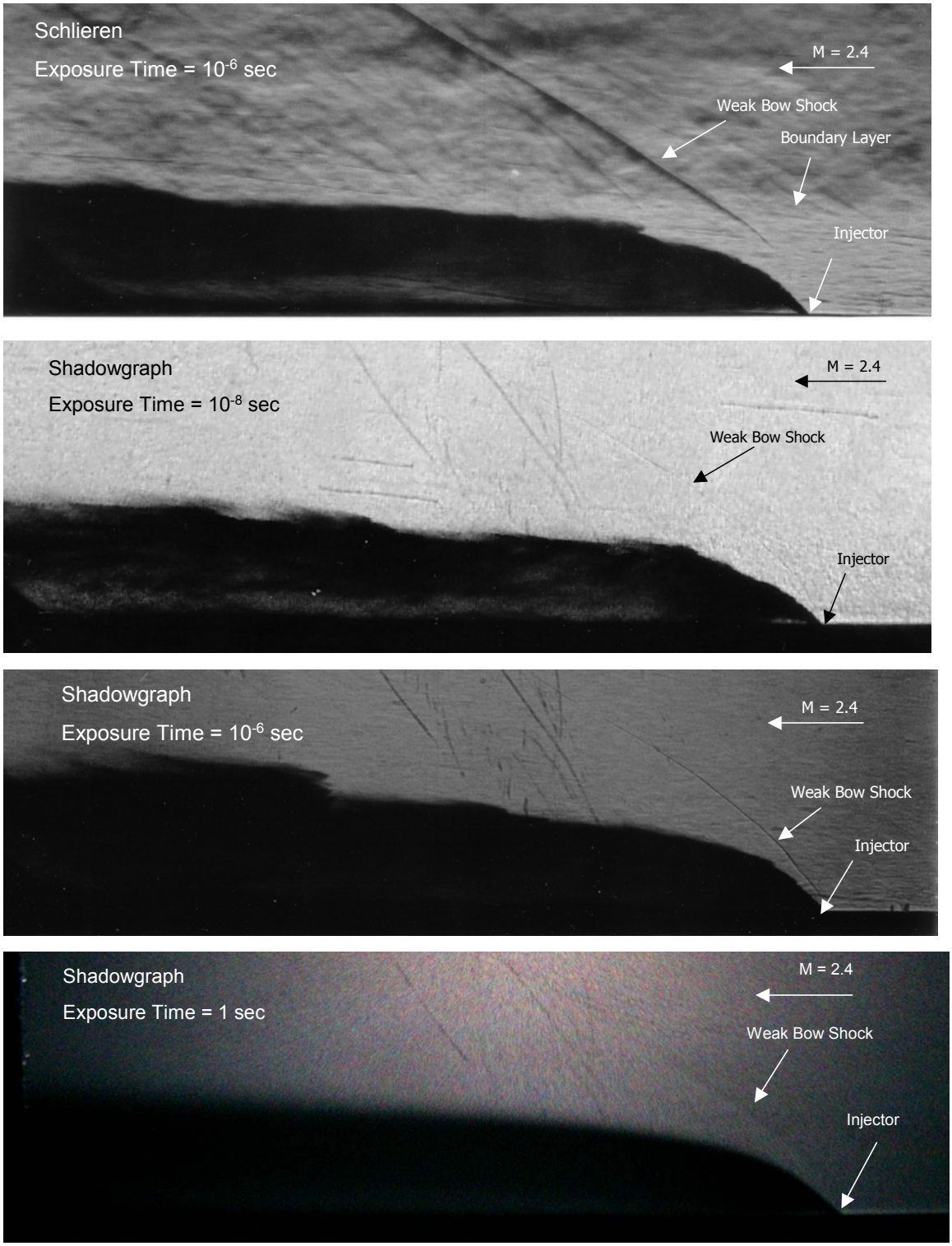

Figure 6.1 Shadowgraph and Schlieren photographs of the liquid injector

The penetration of the injector was measured using the bottom photograph in Figure 6.1. The penetration was measured directly off the photograph as the outer boundary of the visible plume in 2.54 mm increments downstream of the injector. A best-fit curve was then placed over the data points to show a general profile of the injector penetration as a function of distance downstream from the injector. The results of this analysis can be found in Figure 6.2.

Lin, Kennedy and Jackson[45] did a study of liquid jet penetration in a supersonic flow for both pure liquid jets and jets that were a combination of liquid and gas. In their study, they compared correlations for measuring penetration height by using shadowgraphs and by using a phase Doppler particle analyzer, PDPA. They analyzed the shadowgraph measurement correlations created by Yates[46], Kush and Schetz[23], and Baranovsky and Schetz[26] for single jets with no yaw. They found that the correlation that Baranovsky and Schetz[26] used was very similar to the correlations as found by Yates[46] and by Kush and Schetz[23] when applied to 90 degree jets. The correlation found by Baranovsky and Schetz[26] is as follows:

$$y / d_{eq} = 1.32 \ \bar{q}^{0.5} \ln \ (1 + 6(x / d_0)) \sin(2\theta / 3) \qquad (6.1)$$

where θ corresponds to the jet injection angle measured from the freestream direction in degrees. Equation 6.1 was then plotted in Figure 6.2 for a single 90 degree jet with no yaw and for one at 40 degrees with no yaw. This equation was chosen for the reasons that the research was carried out in the same supersonic wind tunnel as in this study, the equation accounts for the angle of the liquid jet, and the penetration was measured using similar techniques to what was used here for measuring the penetration of the liquid aeroramp.

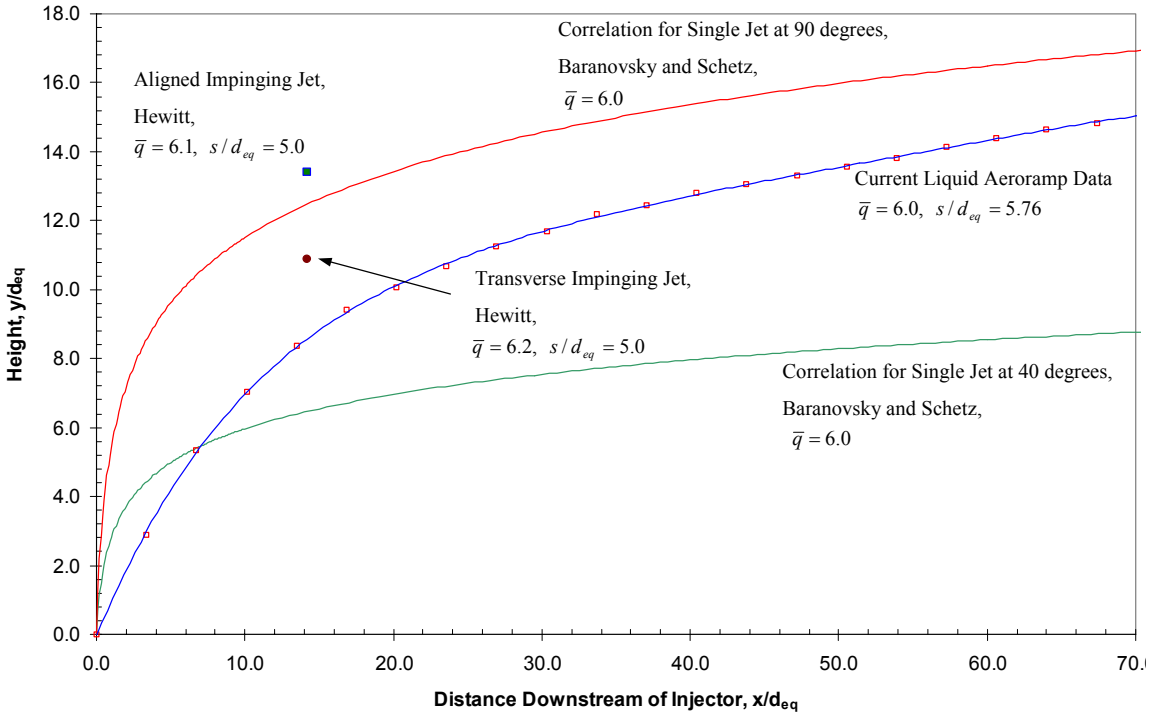

Figure 6.2 Penetration of the liquid injector as a function of distance downstream from the injector

In Figure 6.2 a comparison is made between the two-jet liquid aeroramp, which is angled 40 degrees downstream with 60 degrees toe in, and the correlation given by Baranovksy and Schetz[26] for a single 40 degree jet. One can notice that the liquid aeroramp has much better penetration downstream of the injector than a single, 40 degree jet. The fact that the jet penetrates considerably more than a 40 degree jet suggests that the liquid fuel aeroramp functions as it was originally intended. By impinging the two jets, a vertical liquid sheet is formed and the fluid tends to penetrate farther into the flow and perhaps the aeroramp portion of the liquid fuel aeroramp is inducing additional vorticity and lifting the liquid plume off the floor of the tunnel. The latter was found for gaseous aeroramp injectors. From Figure 6.2 one can see that the liquid fuel aeroramp does not behave as a single 40 degree liquid jet and so one cannot use current liquid jet relations to predict the effect of the downstream angle on the penetration.

Figure 6.2 also shows a comparison between the penetration of the liquid fuel aeroramp at $\bar{q} = 6.0$ and the impinging jet research done by Hewitt[30] for $\bar{q} = 6.1$ and 6.2. The penetration measurement by Hewitt[30] was done at 20 jet diameters or 14.1 equivalent

jet diameters for the two jet system that Hewitt[30] used. In the aligned impinging jet case of Hewitt[30], the front jet is angled 60 degrees downstream with the flow while the back jet is angled 60 degrees into the direction of the flow or 120 degrees with respect to downstream. In the transverse case of Hewitt[30] the impinging jets are aligned perpendicular to the flow. One can notice that the impinging jets by Hewitt[30] in fact penetrate farther in the flow than the liquid fuel aeroramp at this location.

The spacing between the impinging jets by Hewitt are also slightly different than the spacing for the liquid fuel aeroramp. The liquid fuel aeroramp spacing was based on direct photographs of the liquid fuel aeroramp, which resulted in a slightly different spacing when compared to Hewitt.[30] This difference in spacing could result in better penetration and smaller droplet sizes, but this is difficult to determine without further research. The liquid fuel aeroramp and the impinging jets are toed in 60 degrees[30] and so the results shown in Figure 6.2 are primarily a function of the downstream angle and the difference in spacing. Based on this information perhaps the downstream angle of the liquid fuel aeroramp should be increased to an angle close to 60 degrees to study the effect of the downstream angle on the penetration of the liquid fuel aeroramp. The spacing of the impinging jets could also be decreased to study the effects of spacing on the penetration and droplet size.

6.2 Droplet Size Measurements

The mean droplet diameter, D_{32}, vertical profiles were studied as a function of distance from the liquid aeroramp injector. The initial locations for droplet measurements were 30, 60, and 90 effective jet diameters downstream from the injector or 17.6, 35.2 and 52.8 mm, respectively. The results of this study can be found in Table 6.1. The values indicated with a dash were illumination profiles that yielded no useful results. These data points were taken on several occasions, but it is believed that there was so much absorption and scattering, due to multiple droplets in a small area, that almost all light was absorbed and no useful data could be obtained. All the droplet size data presented includes the correction for multiple scattering discussed in Sect. 5.2.1. In correcting the droplet data it was found that as the transmission decreased to 9% the intensity correction in turn increased the droplet size by as much as 11 microns. From

Table 6.1 it can be seen that the droplet diameter ranged from 21 to 33 microns. As the height increased, the droplet size first increased, but the droplet size again decreased towards the edge of the plume. These values are consistent with the values reported by Hewitt[30] for his impinging jet injector for $x / d_{eq} \leq 50$. However, for distances farther downstream it appears as if the impinging jet by Hewitt[30] resulted in smaller droplets than the liquid aeroramp. It seems as if the liquid aeroramp behaves similar to a single 90 degree circular jet in that the droplet size does not appear to fluctuate very much as the distance from the injector increases.[30] Based on this information, it was decided that perhaps a distance farther downstream would have better atomization and thus smaller droplets. The next set of data was then chosen to be recorded at 76.2 mm or 130 effective jet diameters from the injector. The results can be found in Table 6.2. As a reference, at 76.2 mm from the injector the penetration height was approximately 15.2 mm. From Table 6.2 one can see that the droplet diameter varies from 22 to 37 microns. Thus, we found that there was little further atomization beyond the initial three stations. The droplet distribution is also shown in Figure 6.3 along with the penetration height of the injector.

Table 6.1 Vertical distribution of D_{32} in microns as a function of distance from the injector

		Distance, mm (x/d_{eq})		
h/d_{eq}	Height, mm	17.6 (23.3)	35.2 (46.7)	52.8 (70.0)
13.5	10.2	21	23	32
10.1	7.6	28	33	--
6.7	5.1	29	--	33
3.4	2.5	27	31	29

Table 6.2 D_{32} in microns as a function of height at a distance of 76.2 mm (x/d_{eq} = 101.1) from the injector

h/d_{eq}	Height, mm	D_{32}, microns
20.2	15.2	22
18.5	14.0	24
16.8	12.7	23
15.2	11.4	--
13.5	10.2	32
11.8	8.9	34
10.1	7.6	34
8.4	6.4	--
6.7	5.1	37
5.1	3.8	33

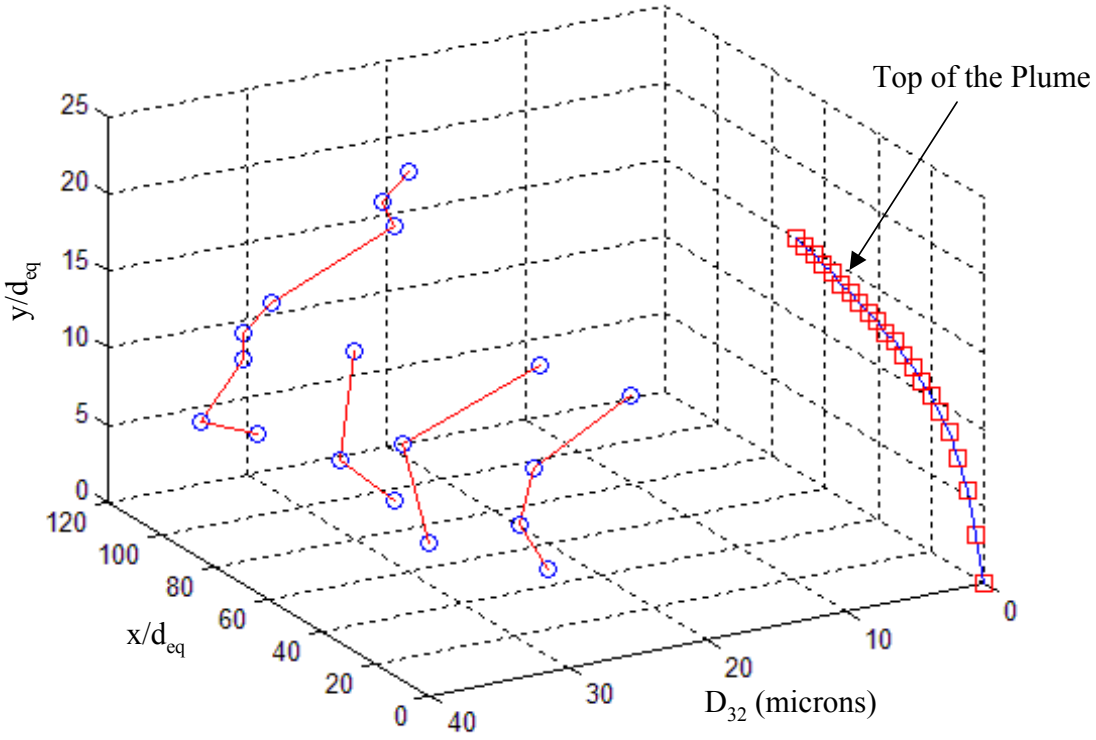

Figure 6.3 Liquid aeroramp penetration and droplet distribution

6.3 Integrated Liquid Aeroramp Injector/Plasma Torch

Initial tests were made using the liquid injector and plasma torch as a combined setup. The plasma torch was set at a distance of 65.4 mm (x/d_{eq} = 86.7) from the injector. This position was simply chosen as a starting point since it was unknown what the best

location would be. As mentioned previously the plasma torch is located almost twice as far from the injector than was used by Jacobsen[21] with the gas injection aeroramp to allow for atomization. The feedstock flowrate of the plasma torch was then set to 25 slpm.

Figure 6.4 shows some results of this testing. One can measure effects due to liquid fuel flow rates, powers, and different feedstocks directly from the photographs by using the case in which $Q_j \approx 1.1$ lpm with the plasma torch power set to approximately 2500 watts as the baseline. In doing these measurements, the maximum distance in both height and width were measured and recorded for each bright plume. The exposure time and f-stop (or f number) are shown in the corner of each photograph in Figures 6.4.

The f-stop (or f number) and exposure time of each photograph can have an effect on the intensity of the bright plume as recorded by the digital camera. This means that changes in the f-stop or exposure time could directly affect any measurements of the height and width of the bright plume. The change in intensity due to changes in *f-stop* and exposure time can be explained by using a few basic relations. By first making the assumption that all of the photographs are taken at approximately the same distance from the liquid fuel injector/plasma igniter one can then relate the intensity as follows:

$$I \propto A\ \Delta t \tag{6.2}$$

where I is the intensity, A is the area of the aperture in the camera, and Δt is the exposure time. The area of the aperture can then be related as:

$$A \propto d_{iris}{}^2 \tag{6.3}$$

where d_{iris} is the diameter of the iris and thus directly related to the aperture. By knowing that the *f-stop* is related by:

$$f - stop = \frac{f}{d_{iris}} \tag{6.4}$$

where *f* is the focal length. Equation 6.4 can then be rewritten as:

$$d_{iris} = \frac{f}{f - stop} \tag{6.5}$$

Therefore, by taking equations 6.3 and 6.5 one can get the following:

$$A \propto (\frac{f}{f-stop})^2 \tag{6.6}$$

Finally, the intensity can be related as:

$$I \propto (\frac{f}{f-stop})^2 \ \Delta t \tag{6.7}$$

From equation 6.7 one can now see how the *f-stop* and time exposure (Δt) are related to the intensity of the bright plume as seen by the digital camera. If one were to fix the focal length then each of these pictures can be repeated based on the *f-stop*. Therefore, all comparisons for the intensity will be made based on the *f-stop* and exposure time alone. By using this intensity relation (Eqn. 6.7) one can now determine the difference in intensity, as recorded by the digital camera, of the bright plume for each of the photographs below.

In looking at Figure 6.4 one should be aware that there is a possibility that oscillations in the plasma torch could be affecting the shape of the bright plume as shown in these particular photographs. Based on past research with this particular plasma torch it is known that the torch oscillates at a frequency of approximately 180 Hz. It is useful to note that the liquid plume oscillates at a high frequency, while the plasma torch oscillates at a low frequency. These oscillations make it difficult to repeat these measurements to get the exact same results as shown here. By looking at the exposure time of each of the photographs, there is a possibility that the bright plume in the $Q_j = 1.074$ lpm photograph is in fact flickering. Since this photograph is used as a baseline it could have an effect on the differences reported for the direct photographs of the integrated liquid aeroramp injector/plasma igniter system.

From Figure 6.4 one can see that the light emanating from the plasma torch appears to increase in width by up to 70% and decrease in height up to 12% as the liquid fuel (kerosene) flow rate decreases. The bright plume also increases in width by 53% and increases in height by 12% as the liquid fuel flow rate increases. It is also useful to note that differences in the f-stop and exposure time can cause an increase in intensity, as seen by the digital camera, of as much as 162% as the liquid fuel flow rate decreases. However, as the liquid fuel flow rate increases the differences in *f-stop* and exposure time can cause a decrease in intensity, as seen by the digital camera, of up to 45%. One

concern here is that we are not seeing combustion, but rather a large amount of scattering of the bright light from the plasma torch by the mist created from the liquid fuel injector. The possibility that the bright light is being scattered along with the flickering of the plasma torch is one explanation as to why there is such a large increase in width of the bright plume as the liquid fuel (kerosene) flow rate varies. In looking at Figure 6.4 one should notice that as the liquid fuel (kerosene) flow rate decreases the bright plume appears to penetrate beyond the edge of the liquid plume. This indicates that the bright plume continues to penetrate into the flow regardless of how low the liquid flow rate is. While, as the liquid fuel flow rate increases the bright plume continues to penetrate into the flow as the penetration of the liquid jet increases. Therefore, it is difficult to say that any combustion is present from these photographs. Of course, it would be surprising if much combustion did occur under these cold-flow, low-pressure conditions.

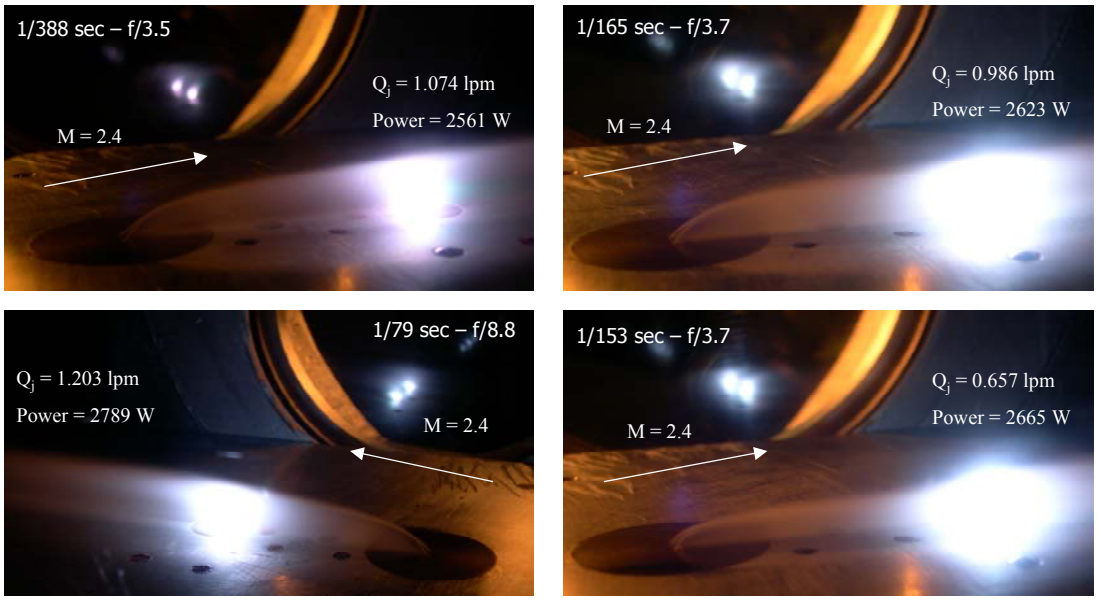

Figure 6.4 Integrated liquid aeroramp injector/plasma torch at varying fuel (kerosene) flow rates using a nitrogen feedstock

Filtered photography was done using an OH filter as described earlier and setting the exposure time on a digital camera to 1 second in order to capture all the light with the same wavelength as OH. The exposure time and focal length are shown in the upper right hand corner of each photograph in Figures 6.5-6.7. Flickering should not be a problem in the OH filtered photographs because of the longer exposure time. The liquid fuel (kerosene) flow rate of the injector is shown in the upper left hand corner along with

the power setting of the plasma torch. The photographs were taken at an angle such that the three dimensional effects of the liquid injector/ plasma torch could be seen. If one were to only take a photograph normal to the injector, then all changes in the plume along the transverse direction would not be seen.

Initially, the liquid fuel (kerosene) flow rate was varied so as to find out what effects the flow rate had on the plume caused by the plasma torch with nitrogen as a feedstock (see Figure 6.5). From Figure 6.5 it can be shown that as the liquid fuel flow rate increases the bright plume increases in height by 30% and increases in width slightly (2%). While, a decrease in flow rate resulted in an increase in height by 9% and an increase in width by 10%. Thus, as the liquid fuel flow rate varies the width and height appear to always increase. This could be explained by looking at the photographs in Figure 6.5 noticing that the shape of the plume changes as the liquid fuel flow rate varies. Another explanation behind this peculiar increase in width and height could be that the anode wears down over time and this could be causing a change in the shape and area of the bright plume. At this point it is difficult to say if any combustion is occurring without more detailed analysis of the bright plume. It is also useful to note that differences in the *f-stop* could cause an increase in intensity of as much as 18% as the fuel flow rate was varied. For the OH filtered photographs the exposure time is the same and thus only the *f-stop* should have an effect on the intensity of the images as recorded by the digital camera.

Once this study was complete, it was decided that the power of the torch should be varied (see Figure 6.6). Again by looking at the photographs, it can be shown that as the plasma torch power decreases the bright plume appears to decrease in width by 9 % and increase in height by 22%. This means that the plume is narrower for lower power settings and appears to penetrate farther into the flow at this lower power setting. This is consistent with the photographs shown in Figure 6.6. It is also useful to note that differences in the *f-stop* could increase the intensity of the bright plume, as seen by the digital camera, of as much as 47% as the torch power decreases.

We then tried air as a feedstock for the plasma torch. While studying the air as a feedstock, the liquid fuel flow rate was varied, as was originally done with the nitrogen feedstock, to see if the air feedstock produced a different reaction to liquid fuel flow rate

variation than the nitrogen feedstock case did (see Figure 6.7). Since there was no difference in the *f-stop* or exposure time there was effectively no difference in intensity of the bright plume as recorded by the digital camera. In studying the air feedstock it was found that the bright plume decreased in height and width slightly (2%) as the liquid fuel flow rate increased. This small change in the plume shape indicates that the plume is only slightly affected by varying the liquid fuel flow rate when using air as the feedstock in the plasma torch. In comparison the nitrogen feedstock photographs show that the bright plume is very much affected by variations in the liquid feedstock flow rate. Comparing the photographs from Figures 6.5 and 6.7, one can make the following observations. The bright plume appears to have better penetration when using the air torch feedstock compared to the nitrogen feedstock. One should note that since both photographs are taken with the same *f-stop* and exposure time there is effectively no difference in intensity as seen by the digital camera. By using air as the feedstock the bright plume appears to increase in width by 19% and increase in height by 17% when compared to nitrogen. Part of this increase in height and width can be attributed to the fact that the air feedstock would not run very well around 2500 watts. Eventually, it was found that the plasma torch was much more consistent at around 3300 watts using air as the feedstock. Several attempts were made to vary the power, but the most useful results occurred around 3300 watts. It is also useful to note that nitrogen lines overlap the OH area when using air as the torch feedstock since air is partially composed of nitrogen.

As mentioned previously it appears as if the bright plume is more affected by the liquid fuel flow rate when using nitrogen as the feedstock than when using air as the feedstock. This observation is made based on the fact that the plume appears to have more curvature in the direction of the flow when using nitrogen as a torch feedstock, than when using air as a torch feedstock. In the photographs with air as a feedstock it appears almost as if the bright plume is completely vertical and thus unaffected by the liquid fuel flow. The bright plume also appears to have sharper edges while the nitrogen feedstock appears to produce a bright plume with much smoother edges. The difference in the shape could be that there are more excited OH molecules around the plume when using air as a torch feedstock than when using nitrogen.

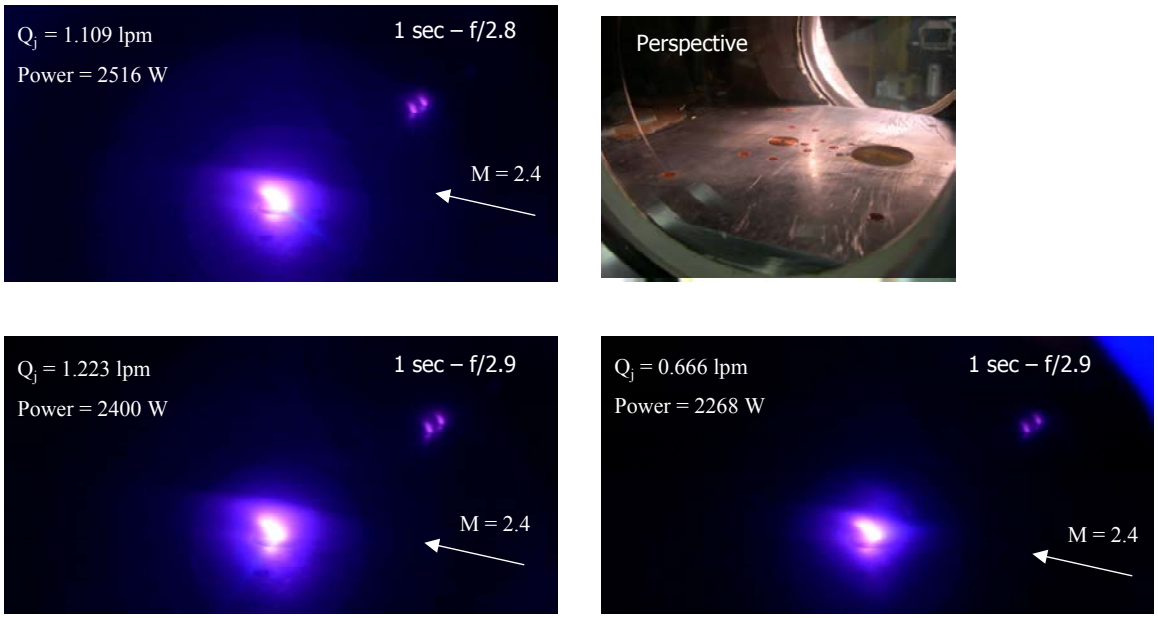

Figure 6.5 OH filtered photographs of liquid aeroramp injector/plasma torch with varying liquid fuel (kerosene) flow rates with nitrogen torch feedstock

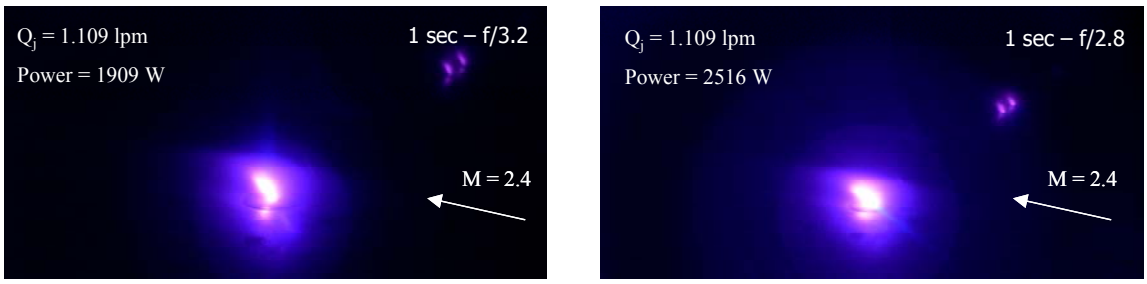

Figure 6.6 OH filtered photographs of liquid aeroramp injector/plasma torch with varying plasma torch power settings with nitrogen torch feedstock and 1.109 lpm of liquid fuel (kerosene)

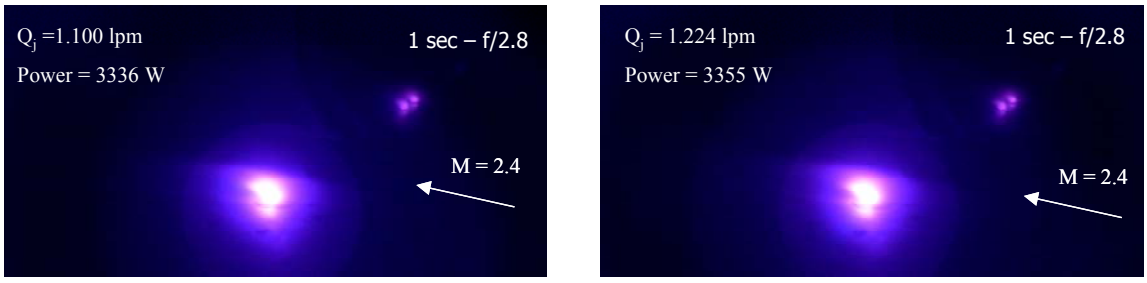

Figure 6.7 OH filtered photographs of liquid aeroramp injector/plasma torch with varying liquid fuel (kerosene) flow rates with air torch feedstock

Chapter 7: Summary and Conclusions

Initial experiments were performed at Virginia Tech to evaluate a new, integrated liquid fuel injection and flameholding device. This new system was comprised of a liquid fuel aeroramp injector, using kerosene as the injectant to simulate JP7 fuel, and a plasma torch for ignition and combustion enhancement. The plasma torch was only initially placed at one location while the liquid fuel flow rate of the injector, power of the plasma torch, and feedstock of the plasma torch were varied.

The plasma torch was operated from 1000 to 5000 watts with nitrogen and air as feedstocks. The torch feedstock flow rate was set at 25 slpm while running chamber pressures between 40 and 50 psig. For the liquid injector/plasma igniter, the plasma torch was initially set at a distance of 65.4 mm from the liquid injector or 112 effective jet diameters from the liquid injector. The liquid aeroramp fuel flow rate was varied from 0.66 lpm to 1.22 lpm during integrated liquid fuel aeroramp/plasma torch testing. The liquid aeroramp was typically run at 1.078 lpm, which corresponds to a momentum flux ratio of 6.0. This liquid fuel flow rate was used for all shadowgraph and schlieren photographs along with a baseline for studying the effects of varying the liquid fuel flow rate, power of the plasma torch, and feedstock of the plasma torch.

The penetration height, shape of the plume, and droplet size were first studied before combining the injector with the plasma torch. This information allowed one to decide on a reasonable initial location for the plasma torch.

Conclusions from the experiment can be summarized. First, the aeroramp liquid injector functions as originally intended. Good penetration and atomization with a weak interaction shock was documented. Second, the liquid fuel flow rate has an effect on the height and width of the bright plume according to the OH wavelength filtered photographs. As the liquid fuel flow rate increases, the bright plume increases in height by 30% and increases in width slightly (2%). While, a decrease in liquid fuel flow rate resulted in an increase in height by 9% and an increase in width by 10%. Thus, as the liquid fuel flow rate varies around the baseline the width and height of the bright plume appear to always increase. This could be explained by noticing that the shape of the bright plume changes as the liquid fuel flow rate varies. Perhaps anode erosion during a test series also plays a part in this variation. The direct photographs of the liquid injector

also show that the liquid fuel flow rate has an effect on the bright plume. Third, from the OH wavelength filtered photographs it was also shown that the bright plume appears to decrease in width by 9% and increase in height by 22% when the plasma torch is set at a lower power setting (1909 W). Fourth, when air is used as the torch feedstock, instead of nitrogen, the bright plume can increase by as much as 19% in width and 17% in height for a liquid fuel volumetric flow rate of 1.1 lpm and plasma torch power of 2516 watts for the nitrogen feedstock and 3336 watts for the air feedstock. Part of this increase in height and width can be attributed to the fact that the air feedstock would not run very well around 2500 W. Fifth, it was found that the plasma torch was much more consistent at around 3300 watts using air as the feedstock. It was also found that the height and width of the bright plume decreased slightly (2%) as the fuel flow rate increased when using air as the torch feedstock. Last, it is difficult to determine if any combustion is present in these cold-flow, low-pressure conditions based on direct photographs or OH filtered photography alone. One concern here is that we are not seeing combustion, but rather a large amount of scattering of the bright light from the plasma torch by the mist created from the liquid fuel injector. Of course, it would be surprising if much combustion did occur under these cold-flow, low-pressure conditions. Testing at hot-flow conditions is needed.

References

[1] Avrashkov, V., Baranovsky, S., and Levin, V., "Gasdynamic Features of Supersonic Kerosene Combustion In a Model Combustion Chamber," AIAA-90-5268, October 1990.

[2] Vinogradov, V., Kobigsky, S., and Petrov, M., "Experimental Investigation of Liquid Carbonhydrogen Fuel Combustion in Channel at Supersonic Velocities," AIAA 92-3429, July 1992.

[3] Mathur, T., Streby, G., Gruber, M., Jackson, K., Donbar, J., Donaldson, W., Jackson, T., Smith, C., and Billig, F., "Supersonic Combustion Experiments with a Cavity-Based Fuel Injector," AIAA 99-2102, June 1999.

[4] Mathur, T., Lin, K.C., Kennedy, P., Gruber, M., Donbar, J., Jackson, T., and Billig, F., "Liquid JP-7 Combustion in a Scramjet Combustor," AIAA 2000-3581, July 2000.

[5] Li, J.G,, Yu, G., Zhang, X.Y., and Huang, Q.S., "Combustion of Kerosene in a Supersonic Stream," AIAA 2000-0615, January 2000.

[6] Situ, M., Wang, C., Lu, H.P., Yu, G., and Zhang, X.Y., "Hot Gas Piloted Energy for Supersonic Combustion of Kerosene with Dual-Cavity," AIAA 2001-0523, January 2001.

[7] Schetz, J.A., Thomas, R.H. and Billig, F.S., "Mixing of Transverse Jets and Wall Jets in Supersonic Flow," in Separated Flows and Jets, V.V. Kozlov and A.V. Dovgal (Edits.), Springer-Verlag, Berlin, 1991.

[8] Schetz, J.A., "Injection and Mixing in a Turbulent Flow," AIAA, New York, New York, 1980.

[9] McClinton, C.R., "The Effect of Injection Angle on the Interaction Between Sonic Secondary Jets and a Supersonic Freestream," NASA TND-6669, February 1972.

[10] Rogers, R.C., "A Study of the Mixing of Hydrogen Injected Normal to a Supersonic Airstream," NASA TN L-7386, Langley Research Center, March 1971.

[11] Barber, M.J., Roe, L.A., and Schetz, J.A., "Simulated Fuel Injection Through a Wedge Shaped Orifice in a Supersonic Flow," AIAA 95-2559, July 1995.

[12] Tomioka, S., Jacobsen, L.S., and Schetz, J.A., "Interaction between a Supersonic Airstream and a Sonic Jet Injected Through a Diamond-Shaped Orifice," AIAA 2000-0088, January 2000.

[13] Lewis, D.P. and Schetz, J.A., "Tangential Injection from Overlaid Slots into a Supersonic Stream," Journal of Propulsion and Power, Vol. 13, No.1, 1997, pp. 59-63, January-February.

[14] Hartfield, R.J., Hollo, S.D. and McDaniel, J.C., "Experimental Investigations of a Supersonic Swept Ramp Injector Using Laser Induced Iodine Fluoresence," *Journal of Propulsion and Power*, Vol. 10, No.1, 1994, pp. 129-135, January-February.

[15] Riggins, D.W. and Vitt, P.H., "Vortex Generation and Mixing in Three-Dimensional Supersonic Combustors," *Journal of Propulsion and Power*, Vol. 11, No. 3, 1995, pp. 419-426, May-June.

[16] Schetz, J.A., and Swanson, R.C., "Turbulent Jet Mixing at High Supersonic Speeds," *Zeitschrift Fuer Flugwissenschaften*, Vol. 21, pp. 166-173, 1973.

[17] Cutler, A.D. and Johnson, C.H., "The Use of Swirling Jets Pairs to Provide Rapid Fuel Penetration in Scramjet Combustors," AIAA 95-0099.

[18] Kraus, D.K., and Cutler, A.D., "Mixing of Swirling Jets in a Supersonic Duct Flow," Journal of Propulsion and Power, Vol. 12, No. 1, 1996, pp. 170-177, January-February.

[19] Jacobsen, L.J., Schetz, J.A., Gallimore, S.D., and O'Brien, W.F., "Mixing enhancement by Jet Swirl in a Multiport Injector Array in Supersonic Flow," FEDSM99-7248, July 1999.

[20] Schetz, J.A., Cox-Stouffer, S. and Fuller, R., "Integrated CFD and Experimental Studies of Complex Injectors in Supersonic Flows," AIAA 98-2780, June 1998.

[21] Jacobsen, L.S., Gallimore, S.D., Schetz, J.A., and O'Brien, W.F., "An Integrated Aeroramp Injector/Plasma-Igniter for Hydrocarbon Fuels in a Supersonic Flow," "Part A: Experimental Studies of the Geometric Configuration," AIAA 2001-1766, April 2001.

[22] Gallimore, S.D ,Jacobsen, L.S., Schetz, J.A., and O'Brien, W.F., "An Integrated Aeroramp Injector/Plasma-Igniter for Hydrocarbon Fuels in a Supersonic Flow," "Part B: Experimental Studies of the Operating Conditions," AIAA 2001-1767, April 2001.

[23] Kush, E.A., Jr. and Schetz, J.A., "Liquid Jet Interaction into a Supersonic Flow," AIAA J., Vol. 11, No. 9, pp. 1223-1224, September 1973.

[24] Joshi, P.B. and Schetz, J.A., "Effect of Injector Geometry on the Structure of a Liquid Jet Injected Normal to a Supersonic Airstream," AIAA J., Vol. 13, No. 9, September 1975.

[25] Schetz, J.A., Kush, E.A., and Joshi, P.B., "Wave Phenomena in Liquid Jet Break-up in a Supersonic Cross Flow," AIAA J., Vol. 18, No. 7, pp. 774-778, July 1980.

[26] Baranovsky, S.I., and Schetz, J.A., "Effect of Injection Angle on Liquid Injection," AIAA J., Vol. 18, No. 6, pp. 625-629, June 1980.

[27] Nejad, A.S. and Schetz, J.A., "Effects of Properties and Location in the Plume on Mean Droplet Diameter for Injection in a Supersonic Stream," AIAA J., Vol. 21, No. 7, pp. 956-961, July 1983.

[28] Nejad, A.S. and Schetz, J.A., "Effects of Viscosity and Surface Tension on a Jet Plume in Supersonic Airstream," AIAA J., Vol. 22, No. 4, pp. 458-459, April 1984.

[29] Less, D., and Schetz, J.A., "Quantitative Study of Time Dependent Character of Spray Plumes," AIAA J., Vol. 24, No. 12, pp. 1979-1986, December 1986.

[30] Hewitt, P.W. and Schetz, J.A., "Atomization of Impinging Liquid Jets in a Supersonic Crossflow," AIAA J., Vol. 21, pp.178, 1983.

[31] Wagner, T.C., O'Brien, W.F., Northam, G.B., and Eggers, J.M., "Plasma Torch Igniter for Scramjets," Journal of Propulsion, Vol. 5, No. 5, 1989. (Originally presented at the 23rd JANNAF Combustion Meeting, 1986)

[32] Barbi, E., Mahan, J.R., O'Brien, W.F. and Wagner, T.C., "Operating Characteristics of a Hydrogen-Argon Plasma Torch for Supersonic Combustion Applications," Journal of Propulsion, vol. 5, No. 2, 1989.

[33] Stouffer, Scott, "Development and Operating Characteristics of an Improved Plasma Torch for Supersonic Combustion Applications," Masters Thesis, Virginia Polytechnic Institute & State University, July 1989.

[34] Potapkin, B, Babaritsky, A., Deminsky, M., Jivotov, V., Smirnov, R., and Rusanov, V., "Plasma Catalysis of Hydrocarbon Reactions in Pulse Microwave Discharge," July 1999.

[35] Masuya, G., Takita, K., Takahashi, K., "Effect of Airstream Mach Number on H_2/N_2 Plasma Igniter," AIAA 2001-0520, January 2001.

[36] Munson, B.R., Young, D.F., Okiishi, T.H., Fundamentals of Fluid Mechanics, 4th edition, John Wiley and Sons, Inc., Copyright 2002, pp. 513-516.

[37] Schetz, J.A., Hawkins, P.F., and Lehman, H., "The Structure of Highly Underexpanded Transverse Jets in a Supersonic Stream," AIAA J., Vol. 5, No. 5, pp. 882-884, May 1967.

[38] Jacobsen, L.S., "An Integrated Aerodynamics-Ramp-Injector/Plasma-Torch-Igniter for Supersonic Combustion Applications with Hydrocarbon Fuels," Virginia Tech, Ph.D. Dissertation, April 2001.

[39] Dobbins, R.A., Crocco, L., and Glassman, I., "Measurement of Mean Particle Sizes of Sprays from Diffractively Scattered Light," AIAA J., Vol. 1, No. 8, August 1963, pp. 1882-1886.

[40] Roberts, J.H. and Webb, M.J., "Measurement of Droplet Size for Wide Range Particle Distributions," AIAA J. Vol. 2 No. 3, March 1964, pp. 583-585.

[41] Mugele, R.A. and Evans, H.D., "Droplet Size Distribution in Sprays," Industrial and Engineering Chemistry, June 1951, pp, 1317-1324.

[42] Dodge, L.G, "Change of calibration of diffraction-based particle sizers in dense sprays," Optical Engineering, Vol. 23 No. 5, September/October 1984.

[43] Hess, C.F. and Trolinger, J.D., "Particle field holography data reduction by Fourier transform analysis," Optical Engineering, Vol. 24 No.3, May/June 1985.

[44] Hirleman, E.D., Oechsle, V., Chigier, N.A., "Response characteristics of laser diffraction particle size analyzers: optical sample volume extent and lens effects," Optical Engineering, Vol. 23 No.5, September/October 1984.

[45] Lin, K.C., Kennedy, P.J., Jackson, T.A., "Penetration Heights of Liquid Jets in High-Speed Crossflows," AIAA 2002-0873, January 2002.

[46] Yates, C.L., "Liquid Injection into a Supersonic Stream," AFAPL-TR-71-97, Vol. 1, Aero Propulsion Laboratory, Wright-Patterson AFB, OH, 1972.

[47] Holman, J.P.,"Design of Experiments," Chapter 16, pp. 638-679, Experimental Methods for Engineers, McGraw-Hill Book Co., N.Y., 2000.

Appendix A: Uncertainties

A.1 Penetration Measurements

The uncertainty in the penetration measurements can be broken up into two pieces. First, a photograph was taken with a screw and Swagelock male/male adapter of known length over top of the injector. A shadowgraph was then taken with the camera in the exact same position. This photograph was then imported into AutoCad and scaled according to the known dimensions of the screw and swagelock adapter such that the shadowgraph would be on a 1:1 scale. Second, the penetration of the liquid jet was estimated using AutoCad and approximating the edge of the liquid plume.

A set of calipers, accurate to 0.0254 mm (0.001 in), was used to measure both the screw and Swagelock adapter. This meant that there was a 0.0254 mm uncertainty in the measurement used to scale the shadowgraphs. By using AutoCad, the boundary of the plume was found to be within ± 0.62 mm. Now going back to the uncertainty in the scaling of the shadowgraph it was found that the scaling could have an effect of up to ± 0.0033 mm on the estimate of the edge of the plume. Therefore, the total standard deviation for the penetration measurements are ± 0.62 mm or $\frac{y}{d_{eq}} = \pm 0.82$.

A.2 Droplet Measurements

The droplet measurement system can be broken down into three major components. These components are the optical equipment, the data acquisition, and the program created to analyze the data. The optical equipment and data acquisition can also be thought of as one component. While the program used to analyze the data can be considered a second component.

During testing much care was taken to reduce as many uncertainties in the optical equipment as possible. These uncertainties include the alignment of the laser, spatial filter, flat mirrors and the plano-convex lens. Each component was carefully aligned so as to keep the laser beam as level as possible while remaining along the optical axis. The alignment was then verified by outlining the laser beam on a piece of cardboard and then moving the cardboard over a large distance to detect any small angle misalignments. It is difficult to quantify any actual uncertainties due to the optical components alone.

The CCD and data acquisition system used in this study was capable of displaying the light intensities to the user in real time. The advantage of this was that one could detect if in fact a lens, tunnel window, or mirror was dirty by looking at the shape and smoothness of the intensity profile. However, it is difficult to detect any misalignments in the optical system by looking at the intensity readings alone. Some adjustment can be made to the optical equipment with the help of the CCD but small misalignments are not easily detected. As far as one can tell there appears to be no alignment problems in the optical system used in this experiment and so any uncertainties due to misalignments in the optical system are considered to be negligible for the purposes of this uncertainty analysis.

Next, a jitter analysis[47] was done of the program used to analyze the data recorded by the CCD. Jitter analysis can be used to study the effects of perturbations to the inputs of a complicated solution or program. In this case the jitter analysis was done by taking $S = S(x_1, x_2, x_3, ...x_n)$ where S is the Sauter mean diameter, also known as D_{32}, and x_n are the inputs required by the program. The sensitivity that the program has to each of these inputs could then be calculated as:

$$\frac{\partial S}{\partial x_n} \approx \frac{S(x_n + \Delta x_n) - S(x_n)}{\Delta x_n} \tag{A.1}$$

for small changes Δx_n. The uncertainty was then calculated as:

$$\delta S = \sqrt{\left[\frac{\partial S}{\partial x_1}\delta x_1\right]^2 + \left[\frac{\partial S}{\partial x_2}\delta x_2\right]^2 + ...\left[\frac{\partial S}{\partial x_n}\delta x_n\right]^2} \tag{A.2}$$

where $\delta S, \delta x_1, \delta x_2, ..., \delta x_n$ are the uncertainties of the calculated D_{32} and the input quantities $x_1, x_2, ..., x_n$. In doing this jitter analysis it was found that the measured droplet calculations have an uncertainty of ± 5 microns. As mentioned in section 5.2.1 the measured droplet sizes were corrected for multiple scattering and absorption and thus a loss in intensity. According to Dodge[42] it is difficult to quantify an exact uncertainty for this correction. Although, Dodge[42] does mention that the correlation used for the droplet size corrections appears to fit the actual data with an R^2 value of roughly 0.92. Based on this information it was decided that the total uncertainty of the corrected

droplets is roughly ± 5 microns assuming that the data has already been corrected for any loss in intensity.

A.3 Plasma Torch Power

The power setting of the plasma torch is difficult to exactly repeat due to anode wear. Because of this variation in torch power it is useful to determine the fluctuation in torch power between different runs. In Figure 6.4 one can show that the torch power increased by as much as 9% as the liquid fuel flow rate varied in the direct photographs. However, when using the OH wavelength filter it was found that the torch power decreased by as much as 10% as the liquid flow rate varied in Figure 6.5. In Figure 6.6 the torch power decreased by 24% while using the OH wavelength filter to study the effect of power on the bright plume. When the feedstock is then changed to air it was found that the power only increased by 1% as the liquid flow rate is varied (see Figure 6.7). Finally, by studying Figures 6.5 and 6.7, for $Q_j \approx 1.1$ lpm, it was found that the torch power increased by 33%. This large difference in torch power is due to the fact that the air feedstock would not run consistently at powers closer to approximately 2500 W.

Vita

Cody Dean Anderson was born on May 24, 1979 in Charleston, West Virginia. He moved to Lyndhurst, Virginia at a very young age where he spent the rest of his youth. Upon completion of High School he spent one year in Germany as part of a student exchange program in which he worked for the DLR in Cologne. He entered Virginia Tech in 1998 where he perused a Bachelors degree followed by a Masters degree in Aerospace Engineering.